Biochimica et Biophysica Acta 1827 (2013) 709–722

Contents lists available at SciVerse ScienceDirect

Biochimica et Biophysica Acta

journal homepage: www.elsevier.com/locate/bbabio

Monogalactosyldiacylglycerol deficiency in tobacco inhibits the cytochrome b_6f-mediated intersystem electron transport process and affects the photostability of the photosystem II apparatus

Wang Wu [a,b], Wenli Ping [a,b], Hanying Wu [a], Minchun Li [a,b], Dan Gu [a], Yinong Xu [a,*]

[a] Key Laboratory of Photobiology, Institute of Botany, Chinese Academy of Sciences, Beijing 100093, China
[b] University of Chinese Academy of Sciences, Beijing 100049, China

ARTICLE INFO

Article history:
Received 30 November 2012
Received in revised form 21 February 2013
Accepted 23 February 2013
Available online 4 March 2013

Keywords:
Monogalactosyldiacylglycerol
Thylakoid membrane
Photosystem II
Cytochrome b_6f
Electron transport
Photoinhibition

ABSTRACT

Monogalactosyldiacylglycerol (MGDG) is the most abundant lipid component of the thylakoid membrane. Although MGDG is believed to be important in sustaining the structure and function of the photosynthetic membrane, its exact role in photosynthesis in vivo requires further investigation. In this study, the transgenic tobacco plant M18, which has an MGDG deficiency of approximately 53%, and which contains many fewer thylakoid membranes and exhibits retarded growth and a chlorotic phenotype, was used to investigate the role of MGDG. Chlorophyll fluorescence analysis of the M18 line revealed that PSII activity was inhibited when the plants were exposed to light. The inactive linear electron transport found in M18 plants was mainly attributed to a block in the intersystem electron transport process that was revealed by P700 redox kinetics and PSI light response analysis. Immunoblotting and Blue Native SDS-PAGE analysis suggested that a reduction in the accumulation of cytochrome b_6f in M18 plants is a direct structural effect of MGDG deficiency, and this is likely to be responsible for the inefficiency observed in intersystem electron transport. Although drastic impairments of PSII subunits were detected in M18 plants grown under normal conditions, further investigations of low-light-grown M18 plants indicated that the impairments are not direct structural effects. Instead, they are likely to result from the cumulative photodamage that occurs due to impaired photostability under long-term exposure to relatively high light levels. The study suggests that MGDG plays important roles in maintaining both the linear electron transport process and the photostability of the PSII apparatus.

1. Introduction

In oxygen-evolving photosynthetic organisms, the thylakoid membrane is the specific site where the light reaction takes place. Through the close cooperation of four important cofactor-protein complexes embedded in the lipid matrix, namely photosystem II (PSII), photosystem I (PSI), cytochrome b_6f ($Cytb_6f$) and ATP synthase (ATPase), thylakoid membranes efficiently convert solar energy to active chemical energy in the form of ATP and NADPH and supply these to the subsequent CO_2 assimilation process that occurs in the chloroplast stroma (in algae and higher plants) or the cytosol (in cyanobacteria) and through which stable chemical energy is finally stored in the form of carbohydrate. It is generally accepted that the thylakoid membrane, which is mainly composed of glycolipids instead of the phospholipids found in other biological membranes, provides an exclusive matrix in which the photosynthetic apparatus is able to sustain its structural and functional integrity. In higher plants, the thylakoid membrane is characterized by high levels of two galactolipids, namely monogalactosyldiacylglycerol (MGDG) and digalactosyldiacylglycerol (DGDG). These account for approximately 50% and 30% of the total thylakoid lipids, respectively, while two other lipids, sulfoquinovosyldiacylglycerol (SQDG) and phosphatidylglycerol (PG), each account for only 5–12% [1–3]. Besides their high abundance in the thylakoid membrane, galactolipids are rich in polyunsaturated fatty acyl chains, which give them unusual biophysical features [4] and enable them to maintain the appropriate fluidity and flexibility of the membrane [2]. In the case of MGDG, a small galactose head group and two acyl chains rich in double bonds, which occupy a larger space, give it a conical molecular shape and a tendency to form the so-called hexagonal H_{II} structure in vitro. In the case of DGDG, however, an additional galactose molecule attached to the head group gives it a cylindrical molecular shape, thus making it well suited to the formation of a bilayer [4]. In fact, MGDG is the only non-bilayer-forming lipid in the thylakoid membrane and is thus considered to be crucial for the organization of a highly stacked thylakoid membrane structure [5]. In addition, crystallographic studies have shown that MGDG is also the most

Abbreviations: PC, phosphatidylcholine; PE, phosphatidylethanolamine; PS, phosphatidylserine; PI, phosphatidylinositol; UDP, uridine diphosphate; Q_A, primary quinone acceptors of photosystem II; PTGS, post-transcriptional gene silencing

* Corresponding author. Tel./fax: +86 10 62836504.
E-mail address: yinongxu@ibcas.ac.cn (Y. Xu).

0005-2728/$ – see front matter © 2013 Elsevier B.V. All rights reserved.
http://dx.doi.org/10.1016/j.bbabio.2013.02.013

abundant integral lipid in the PSII complex [6,7] (the so-called "functional lipids" [2]), and this may be an essential factor in several processes, such as PSII monomer–monomer interactions and the PSII repair process (for recent reviews, see [8,9]).

In seed plants, the biosynthesis of MGDG exclusively occurs in plastids, and its final step is catalyzed by MGDG synthase (EC 2.4.1.46, UDP-galactose: 1, 2-diacylglycerol 3-β-D-galactosyltransferase), which transfers galactose from UDP-galactose to diacylglycerol (DAG) [10,11]. Although three functional MGDG synthases [MGD1 (A-type), MGD2 and MGD3 (B-type)] have been identified in the model plant *Arabidopsis thaliana*, MGD1, encoded by the *AtMGD1* gene, is considered to be predominantly responsible for the biosynthesis of the bulk of the MGDG synthesized during thylakoid membrane biogenesis in green tissues [12,13]. The significance of MGDG in maintaining the structural and functional integrity of the thylakoid membrane in vivo has been substantiated by studies of two Arabidopsis MGD1 mutants. In the *mgd1-1* mutant [14], which has an MGDG deficiency of approximately 42%, the chloroplasts were severely underdeveloped and contained fewer internal thylakoid membranes, especially the grana lamellae. In addition, the *mgd1-1* mutant was found to contain about 50% less chlorophyll per plant than was found in wild type plants, and this deficiency was responsible for its chlorotic phenotype. Analysis of *mgd1-2* [15], a null mutant in which MGDG and DGDG are almost absent, revealed that the development of photosynthetic membranes almost completely fails in these plants and no chlorophyll or PSII proteins accumulate, leading to the loss of both photosynthetic activity and photoautotrophic ability. Nevertheless, compared with DGDG, whose roles in photosynthesis have been extensively investigated using the *dgd1* mutant [16] and the *dgd1 dgd2* double mutant [17] (for reviews, see [3,18]), our understanding of the exact roles of MGDG in photosynthetic activities is limited at present. It is impossible to address this issue by studying the *mgd1-2* mutant due to the disorganization of the thylakoid membranes that is a characteristic of this mutant line. Aronsson et al. [19] investigated the photosynthetic properties of *mgd1-1* and suggested that a 42% deficiency of MGDG in Arabidopsis has no impact on photosynthetic efficiency or the accumulation of photosynthetic proteins in low-light-grown plants, though the mutant was more susceptible to light stress. Although obtaining viable mutants with greater MGDG deficiencies would be of significant benefit to further investigations, isolating such mutants would be problematic because it is difficult to control the extent of the MGDG knockdown that results from genetic manipulation. Moreover, severe lipid mutants, especially of dwarfish Arabidopsis plants, always have survival difficulties.

Thanks to the broad evolutionary conservation and distribution of the A-type MGDG synthase in plant species and its predominant role in MGDG biosynthesis in green tissues, it is possible to expand our understanding of the role of MGDG in photosynthesis by studying other plants. We previously identified several transgenic tobacco lines with MGDG deficiencies that resulted from post-transcriptional gene silencing (PTGS) of *NtMGD1* [20]. In this study, a well-established transgenic plant line, designated as M18, with about 53% MGDG deficiency was utilized to investigate the role of MGDG in sustaining photosynthetic structure and function in vivo. Like Arabidopsis, tobacco has been shown to be a typical "16:3 plant" [21], which means that both the prokaryotic pathway (characterized by a 16-C fatty acid at the sn-2 position in the MGDG molecule) and the eukaryotic pathway (characterized by an 18-C fatty acid at the sn-2 position in the MGDG molecule) are involved in MGDG biosynthesis [22]. This means that, to some extent, it is reasonable to discuss our results in parallel with those obtained previously in Arabidopsis. The MGDG deficiency of greater than 50% that is found in the M18 line is expected to provide us with significant new insight into MGDG function.

Investigation of the *mgd1-1* mutant showed that low-light-grown mutant plants suffered from increased PSII photoinhibition compared with wild type plants when subjected to a short-term high light treatment [19]. As photoinhibition always involves the loss of active PSII centers, which need to be recovered by degradation and synthesis of the D1 protein [23], the increase in PSII photoinhibition seen in the mutant plants implies that MGDG may play an important role in maintaining the photostability of the PSII apparatus. In this respect, it would be advisable to take the photoinhibition event into account when investigating photosynthesis in MGDG-deficient plants, especially when different light intensities are used for growth. In the present study, photoinhibition was a major focus and was considered to be an important factor in distinguishing between the direct and indirect effects of MGDG deficiency in M18 tobacco.

2. Materials and methods

2.1. Plant materials and growth conditions

Wild type (WT) common tobacco (*Nicotiana tabacum* L. cv. Wisconsin-38) was used as the control plant in this study. WT and T_0 generation M18 plants were maintained by micropropagation on 0.8% solidified agar containing half-strength Murashige and Skoog medium (pH 5.8) supplemented with 3% sucrose. Seedlings in flasks were grown in a growth chamber at 28 °C (daytime) and 26 °C (nighttime) with a light intensity of approximately 60 μmol m^{-2} s^{-1} under a photoperiod of 14 h light/10 h dark. For examination of tobacco plants grown under normal conditions, 3- to 4-week-old seedlings were transferred to soil and grown for another 4 weeks in a greenhouse at 25–28 °C under controlled light conditions with a maximum daily light intensity of approximately 500 μmol m^{-2} s^{-1} at noon in a natural photoperiod. To examine the tobacco plants grown under low light conditions, 3- to 4-week-old seedlings were transferred to soil and grown for another 2 weeks with a light intensity of 100 μmol m^{-2} s^{-1} and with all other conditions maintained as described for seedlings grown in the growth chamber. Unless otherwise stated, all measurements were carried out using the fully expanded leaves (fourth or fifth leaves from the top) of the tobacco plants.

2.2. RNA extraction, isolation of NtMGD2 cDNA and RT-PCR analysis

Total RNA was extracted from the tobacco leaves using a Transzol reagent kit (TransGen Biotech Co., Ltd., Beijing, China) in accordance with the manufacturer's instructions. After treatment with DNase I to eliminate any DNA contamination, 3–5 μg of total RNA from each sample was used as the template for first strand cDNA synthesis by the M-MLV reverse transcriptase (Promega, USA). To isolate an *NtMGD2* cDNA fragment, several B-type *MGD* cDNA and EST sequences identified in a database (*A. thaliana MGD2*, NM_122048; *A. thaliana MGD3*, NM_126865; *Vigna unguiculata*, EF466098; *Glycine max*, AW666268) were aligned and the following degenerate PCR primers were designed: sense, 5′-ATGCAR(A/G)CAY(C/T)ATW(A/T)CCATTGTG-3'; antisense, 5'-TCACAR(A/G)GCTCCCATCCAT-3'. A partial *NtMGD2* sequence was obtained by PCR amplification and 3' rapid amplification of cDNA ends (3'-RACE) [24] was then carried out. For RT-PCR analysis of *NtMGD1* and *NtMGD2* transcript levels, specific primers were designed as follows: *NtMGD1*-sense, 5'-ACTCAAGAACCCACTAACCC-3'; *NtMGD1*-antisense, 5'-CTGTCCAGCAATGTAATCAT-3'; *NtMGD2*-sense, 5'-CATTGTGGGTTCTTAAATGG-3'; *NtMGD2*-antisense, 5'-GGAATGTTTGCAAGTGGACC-3'. The expression level of a tobacco *ACTIN* was used as the internal control and the primer sequences used were as follows: *ACTIN*-sense, 5'-CCCTCCCACATGCTATTCT-3'; *ACTIN*-antisense, 5'-AGAGCCTCCAATCCAGACA-3'.

2.3. Lipid extraction and fatty acid analysis

Lipid extraction was carried out in general accordance with an established protocol [25] but with minor modifications. For total fatty acid analysis, a moiety of the lipid extract was directly

transesterified by reaction with 5% H_2SO_4 in methanol at 85 °C for 1 h, after which it was re-extracted using hexane and subjected to gas chromatography (GC) analysis. For the analysis of membrane lipids, the lipid extract was separated into its individual lipid components by two-dimensional silica gel thin layer chromatography using the following solvent systems: chloroform/methanol/water (65:25:4, v/v/v) for the first dimension, and chloroform/methanol/ammonia (65:35:5, v/v/v) for the second dimension. The lipid spots were visualized under 365 nm UV light after spraying the plate with 0.01% primuline (Sigma, USA) in an acetone/water (60:40, v/v) mixture. The spots were then scraped into glass tubes individually and subjected to transesterification followed by GC analysis. GC analysis of fatty acid methyl esters was carried out in accordance with an established protocol [26]. Heptadecanoic acid (17:0) was used as the internal standard in all quantitative measurements.

2.4. Pigment extraction and HPLC analysis

Pigments were extracted and analyzed in general accordance with an established protocol [27] but with minor modifications. HPLC was performed with a C-18 reversed-phase column (Alltima C18, 5 μm particle size, 250 mm × 4.6 mm, Grace, USA) equipped in a Waters Millennium 2010 apparatus. The pigments were separated with the following elution profile: 100% solvent I (acetonitrile:methanol, 75:25, v/v) for the first 9 min followed by a 2.5 min linear gradient to 100% solvent II (methanol:ethylacetate, 70:30, v/v) which was then continued isocratically until the end of the 30 min separation period. The flow rate was 1 ml min^{-1}. The column was re-equilibrated with solvent I for 10 min prior to the next injection. The pigments were detected by their absorbance at 445 nm.

2.5. Preparation of mesophyll cells for chloroplast counting

To obtain intact mesophyll cells for chloroplast counting, leaf tissues were macerated in accordance with a previously published protocol [28]. Strips sliced from tobacco leaves were fixed in 3.5% glutaraldehyde for 1 h in the dark. After fixation, the material was incubated in 0.1 M Na_2EDTA (pH 9.0) and shaken violently during incubation at 60 °C for 2 h. The dissociated mesophyll cells were observed under Nomarski differential interference contrast optics and the number of chloroplasts per cell was counted and analyzed statistically.

2.6. Transmission electron microscopy

To examine the ultrastructure of plastids, tobacco leaves were cut into small pieces and fixed immediately in 3% glutaraldehyde in 0.1 M phosphate buffered saline (PBS, pH 7.2) for 4 h at room temperature and overnight at 4 °C. After fixation, the specimens were rinsed three times with PBS and postfixed in 1% OsO_4 in the same buffer overnight at 4 °C. After being rinsed three times with PBS and dehydrated in an acetone series at room temperature, the specimens were infiltrated with a graded concentration series of epoxy resin in epoxy propane. The specimens were then embedded in Spurr resin which was subsequently polymerized by heating. Ultrathin sections (70 nm) were obtained using a Leica Ultracut R (Germany) and stained with uranyl acetate followed by lead citrate. The sections were viewed with a transmission electron microscope (JEM 1230, JEOL, Japan).

2.7. Photosynthetic measurements

2.7.1. Modulated chlorophyll a fluorescence analysis

In vivo chlorophyll a fluorescence was measured using a PAM-2000 portable chlorophyll fluorometer (Heinz Walz, Effeltrich, Germany) connected to a leaf-clip holder (Model 2030-B, Heinz Walz, Germany). The whole procedure was performed in a dark room at 25 °C under stable ambient conditions. Before measurement, the plants were dark-adapted for 30 min. The minimum chlorophyll fluorescence at open PSII centers in the dark (F_o) and under actinic light (F_o') was determined using a weak, red measuring light (650 nm) with very low intensity (0.8 μmol m^{-2} s^{-1}). A saturating pulse of white light (3000 μmol m^{-2} s^{-1} for 800 ms) was applied in order to estimate the maximum chlorophyll fluorescence at closed PSII centers in the dark (F_m) and under actinic light (F_m'). The steady-state chlorophyll fluorescence (F_s) was recorded during actinic light illumination. The maximal photochemical efficiency of PSII (F_v/F_m) was calculated as $(F_m - F_o)/F_m$. The actual PSII efficiency (ΦPSII) was calculated as $(F_m' - F_s)/F_m'$. The photochemical quenching (qP) and the non-photochemical quenching (NPQ) were calculated as $(F_m' - F_s)/(F_m' - F_o')$ and $(F_m - F_m')/F_m'$, respectively. The actinic light intensities utilized in determining the light response curve were 11, 60, 100, 170, 270, 420, 600, 970, 1410 and 2110 μmol m^{-2} s^{-1} in sequence.

2.7.2. Measurement of P700 redox kinetics and PSI light response curves

Measurement of light-induced P700 absorbance changes at 820 nm was performed using a PAM-101 fluorometer connected to an ED 800 T emitter–detector unit (Heinz Walz, Germany) and mainly in accordance with a previously published protocol [29]. Leaf discs of equal area from dark-adapted plants were first subjected to actinic light irradiation (100 μmol m^{-2} s^{-1}) for 60 s, after which the relative amount of P700 (ΔA) was estimated. Far-red light (720 nm, 24 μmol m^{-2} s^{-1}) exposure was then used to selectively oxidize P700 molecules. Maximum oxidation of P700 was obtained using a saturating white light pulse (3000 μmol m^{-2} s^{-1} for 800 ms) superimposed onto the far red light background to provide a measure of the relative amount of total photooxidizable P700 (ΔA_{max}). Following the pulse, the PSII-dependent $P700^+$ re-reduction process was monitored as a negative absorbance peak reflecting the intersystem electron transport activity. PSI light response curves were recorded using a Dual-PAM-100 measuring system in accordance with a previously published method [30]. Basic fluorescence parameters including maximal (Pm, Pm'), steady state (P) and zero (Po) P700 signal levels were first determined under each defined actinic light intensity with a 30 s adaptation period during a series of stepwise increases in intensity (6, 13, 37, 53, 95, 166, 273, 339, 660, 1028, 1594 and 1952 μmol m^{-2} s^{-1} in sequence). The quantum yield of photochemical energy conversion [Y(I)], the quantum yield of non-photochemical energy dissipation due to donor side limitation [Y(ND)] and the quantum yield of non-photochemical energy dissipation due to acceptor side limitation [Y(NA)] were calculated automatically by Dual-PAM software.

2.7.3. Low temperature (77 K) chlorophyll fluorescence

77 K chlorophyll fluorescence measurements of thylakoid preparations were performed using an F-4500 fluorescence spectrophotometer (Hitachi, Japan) with chlorophyll a excited at 436 nm. The chlorophyll concentration in the thylakoid preparations was adjusted to 5 μg ml^{-1}. Fluorescence emission spectra were recorded from 600 nm to 800 nm and normalized to the PSI peak centered at approximately 730 nm.

2.7.4. Measurement of oxygen evolving activity

The oxygen evolving activities of the freshly extracted thylakoid membranes were measured with a Clark-type electrode (Hansatech, UK) at 30 °C under saturating light (3900 μmol m^{-2} s^{-1}). The chlorophyll concentration in the thylakoid preparations was adjusted to 15 μg ml^{-1} and the measurements were carried out in a buffer containing 400 mM sucrose, 10 mM NaCl, 5 mM $MgCl_2$, 1 mM Na_2EDTA and 10 mM HEPES-NaOH (pH 7.5) that was supplemented with 5 mM NH_4Cl as an uncoupler. PSII oxygen evolving activity was measured in the presence of 1 mM 2,6-dichloro-p-benzoquinone (DCBQ), which acts as an artificial electron acceptor, and with 1 mM potassium ferricyanide [$K_3Fe(CN)_6$] added to keep the quinones in the oxidized form. Whole-chain oxygen evolving activity was measured in the presence of 2 mM $K_3Fe(CN)_6$ as an electron acceptor [31].

2.8. Total protein extraction, SDS-PAGE and immunoblotting analysis

Total proteins were extracted from tobacco leaves in general accordance with a previously published protocol [32] with minor modifications, and the protein concentration was determined using the Bio-Rad DC protein assay (Bio-Rad, USA). Protein samples were separated in 15% SDS polyacrylamide gels containing 6 M urea [33], which were then stained with 1% Coomassie Brilliant Blue R250 to evaluate the variation in loading amongst the samples. For immunoblotting analysis, the total protein samples were separated by SDS-PAGE or Tricine-SDS-PAGE [34] (for PsaC) and were electrotransferred to nitrocellulose membranes (Amersham Biosciences, USA) before being incubated with specific primary antibodies. The signal from the HRP-conjugated secondary antibody was detected using the enhanced chemiluminescence method in accordance with a standard protocol. All antibodies used in this study were rabbit polyclonal antibodies. Rabbit antibodies against D2, LHCII, PsbO, PsaA/B, Cytf, CF1β, the large subunit of Rubisco (RbcLS) and Ferredoxin: $NADP^+$ reductase (FNR) were kindly provided by Dr. Lixin Zhang (Institute of Botany, CAS, China). Rabbit antibodies against CP43, CP47 and Rubisco activase (RCA) were kindly provided by Dr. Congming Lu (Institute of Botany, CAS, China). All other antibodies were purchased from AgriSera (Vännäs, Sweden).

2.9. Thylakoid membrane preparation

Thylakoid membranes were prepared using a previously published protocol [35] with minor modifications. Briefly, leaves were homogenized in an ice-cold isolation buffer (400 mM sucrose, 10 mM NaCl, 2 mM $MgCl_2$, and 50 mM HEPES-KOH, pH7.8) before being filtered through four layers of cheesecloth and centrifuged at 300 ×*g* for 5 min to remove the residual debris. The supernatant was centrifuged at 5000 ×*g* for 10 min to deposit the thylakoid membranes. The pellets were washed several times with isolation buffer to remove starch particles and were suspended in the same buffer. The whole procedure was conducted at 4 °C under darkened conditions. The chlorophyll concentration was determined using a previously published method [36]. The preparations were either used immediately or frozen in liquid nitrogen and stored at −70 °C until use.

2.10. Blue Native PAGE (BN-PAGE), SDS-PAGE and protein identification

BN-PAGE was carried out using an established protocol [35] with minor modifications. Thylakoid membranes were washed twice with resuspension buffer (20% glycerol and 25 mM Bis-Tris HCl, pH 7.0) and solubilized in a solution of 1% (w/v) dodecyl-β-D-maltopyranoside (DM) in resuspension buffer before bringing the samples to a final chlorophyll concentration of 0.5 mg ml^{-1}. After incubation on ice for 10 min, the insoluble material was removed by centrifugation at 12,000 ×*g* for 10 min. The supernatant was then combined with a 0.1 volume of loading buffer [5% (w/v) Serva Blue G, 100 mM Bis-Tris HCl (pH 7.0), 0.5 M 6-amino-n-caproic acid, 30% (w/v) glycerol] and loaded onto a 0.75 mm thick 5%–12% acrylamide gradient BN-gel. For two-dimensional separations, excised BN-PAGE lanes were soaked in SDS sample buffer containing 5% β-mercaptoethanol for 1 h and then layered onto 1 mm thick 15% SDS polyacrylamide gels containing 6 M urea. For protein identification, protein spots sliced from the gels were pretreated and in-gel digested by trypsin in accordance with a previously published protocol [37] and then identified using a MALDI-TOF-TOF mass spectrometer (UltrafleXtreme, Bruker Daltonics, Billerica, MA, USA). Mass spectrometry (MS) data were uploaded to Mascot on the Matrix Science public website (http://www.matrixscience.com) using Biotools software (Ver. 3.2, Bruker Daltonics) and used to query the NCBI nr protein database (Version 20120722, 19256848 sequences, 6606790375 residues).

2.11. Photoinhibition and recovery treatment

Detached leaf disks from tobacco plants grown for two weeks under low light conditions (100 μmol m^{-2} s^{-1}) were first incubated either in water or in 1 mM lincomycin solution (to block the de novo synthesis of chloroplast-encoded proteins) under darkened conditions for 3 h. After incubation, the initial F_v/F_m values were determined at the 0 h time point. Then, leaf disks floating adaxial side up were subjected to 500 μmol m^{-2} s^{-1} irradiation and the F_v/F_m values at 1 h, 2 h and 4 h were recorded. After 4 h of continuous irradiation, the leaf disks were allowed to recover under dim light while the F_v/F_m values were recorded at various timepoints. Throughout this procedure, the temperature was maintained at approximately 25 °C. To estimate the photostability of the PSII proteins, changes in the PSII protein content of WT and M18 plant tissues during photoinhibition were assayed by immunoblotting.

3. Results

3.1. MGDG deficiency leads to a greatly changed lipid profile and causes a chlorotic phenotype in M18 tobacco plants

Stable silencing of the *NtMGD1* gene in M18 plants during various growth periods and under diverse physiological conditions was confirmed by RT-PCR analysis (data not shown). To exclude the possibility that non-specific gene silencing and/or complementary expression of B-type MGDG synthase genes not yet reported in tobacco occur alongside *NtMGD1* silencing, we isolated an *NtMGD2* cDNA fragment and examined its expression levels by RT-PCR. Fig. 1 shows the results of comparative analysis of *NtMGD1* and *NtMGD2* mRNA abundance in leaves from different positions in WT and M18 plants grown for 4 weeks in the greenhouse. In M18 plants, *NtMGD1* transcripts were found to be depleted in young, mature and old leaves represented by N2, N5 and N8 [numbered from the apical bud (N1) of the plant], respectively, while *NtMGD2* transcript levels were not affected. As a result of specific inhibition of *NtMGD1* expression, the relative abundance of MGDG among the total membrane lipids in M18 mature leaves was about 53% lower than that in WT leaves (Fig. 2A). Concomitantly, the relative abundance of the nonchloroplastic lipids PC, PE and PS/PI was significantly increased in M18, whereas, interestingly, the levels of other chloroplastic lipids DGDG, PG and SQDG were not significantly affected (Fig. 2A). As a consequence, the ratio of chloroplastic lipids to nonchloroplastic lipids (CL/NCL) and the ratio of non-bilayer-forming lipids to bilayer-forming lipids [MGDG/(DGDG + PG + SQDG)] in plastids were both significantly reduced in M18 (Fig. 2B). Total fatty acid analysis indicated that, in spite of the loss of MGDG, the total lipid content (fatty acid weight per dry weight, mg/g) in the leaves of M18 plants was not significantly different from that of WT plants (56.41 ± 0.33 mg/g and 61.08 ± 1.17 mg/g, respectively). However, the defect in MGDG greatly reduced the levels of polyunsaturated fatty acids (18:3 and 16:3) in M18 leaves (Fig. 2C). In particular, the level of 16:3 was reduced by more than 80% because of its almost

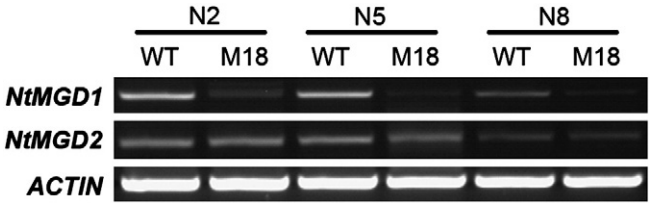

Fig. 1. RT-PCR analysis of *NtMGD* gene transcript levels in the leaves of WT and M18 plants grown under normal conditions. N2, N5 and N8 indicate the leaf positions numbered from the apical bud (N1) of tobacco plants, which represent young, mature and old leaves, respectively. Total RNA was extracted from leaves and the expression levels of *NtMGD1* and *NtMGD2* were determined by RT-PCR with 30 amplification cycles. *ACTIN* was used as a control.

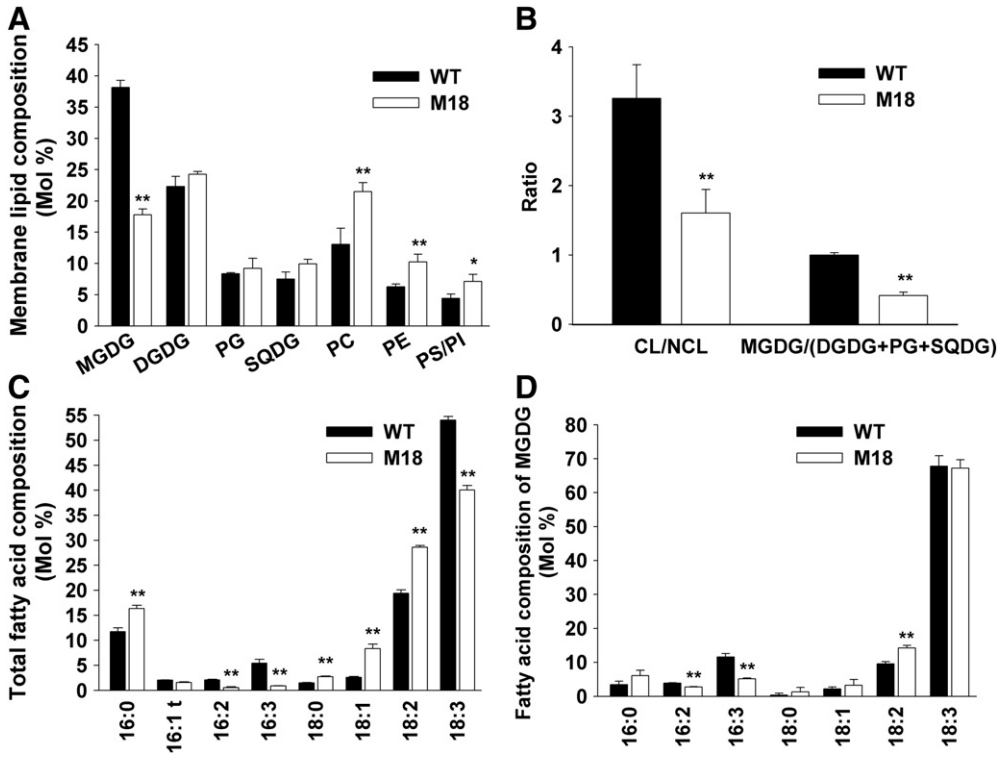

Fig. 2. Lipid profile comparison of leaves from WT plants (filled bars) and M18 plants (open bars) grown under normal conditions. A, Membrane lipid composition of WT and M18 leaves. PC, phosphatidylcholine; PE, phosphatidylethanolamine; PS, phosphatidylserine; PI, phosphatidylinositol. PS/PI indicates data from either of the two lipids or from both, due to the low resolution of the two lipid components on the TLC gel. B, Ratios of chloroplastic lipids (CL) to nonchloroplastic lipids (NCL) and MGDG to (DGDG + PG + SQDG) calculated from the data shown in panel A. CL include MGDG, DGDG, PG and SQDG; NCL include PC, PE and PS/PI. MGDG/(DGDG + PG + SQDG) represents the ratio of non-bilayer-forming lipids to bilayer-forming lipids in plastids. C, Total fatty acid composition of lipid extracts from WT and M18 plants. 16:1 t, trans-Δ^3-hexadecenoic acid. D, Fatty acid composition of MGDG from WT and M18 plants. All values are means ± SD from three independent measurements. Student's t-test was performed and the asterisks indicate statistically significant differences between WT and M18 samples (*, $P < 0.05$; **, $P < 0.01$).

exclusive existence in MGDG. Fatty acid composition analysis of MGDG revealed a major deficiency in 16:3 but not in 18:3 in M18 plants (Fig. 2D), which indicates that the lack of MGDG biosynthesis in M18 plants could be mainly attributable to a suppression of the prokaryotic biosynthetic pathway similar to that revealed in the Arabidopsis *mgd1-1* mutant [14].

Under normal growth conditions, M18 plants exhibit retarded growth and a chlorotic phenotype (Fig. 3A). Determination of pigment composition (Fig. 3B) revealed that the total pigment content (nmol per fresh weight, nmol/g) in the developed leaves of M18 plants was approximately 36% lower than that of WT plants, due to comparable reductions in the levels of chlorophylls and carotenoids. In the case of the chlorophylls, the Chl a content of M18 leaves was found to be reduced by approximately 31% relative to WT, while a much greater reduction was detected in the level of Chl b (approximately 50%). As a result, the Chl a/Chl b ratio in M18 was greatly increased (3.77 ± 0.06 in M18 versus 2.71 ± 0.02 in WT). Similarly, the levels of the carotenoids neoxanthin (N), lutein (L) and β-carotene, together with the sum of the levels of the xanthophyll-cycle pigments violaxanthin and antheraxanthin (zeaxanthin was found in trace amounts and not counted), were all found to be significantly reduced in M18 leaves, where the reductions observed were approximately 56%, 49%, 21% and 17%, respectively.

3.2. Chloroplast development and internal membrane structure are impaired in M18 plants

The reduced proportion of chloroplastic lipids found in M18 plants implies a possible defect in the chloroplast membrane system, and the large decrease in the levels of non-bilayer-forming lipids in plastids was expected to affect the architecture of the thylakoid membrane. To assess these possibilities, the morphology of the chloroplasts in developed leaves from WT and M18 plants were first compared by differential interference microscopy (Fig. 4A). Many fewer chloroplasts were present in M18 leaves than in WT leaves, both in the palisade mesophyll cells and in the spongy parenchyma cells, while the chloroplasts in the M18 leaves seemed slightly larger than those in the leaves of WT plants. Statistical analysis showed that the chloroplast number per cell in the M18 leaves was approximately 60% lower than that found in WT leaves (Fig. 4B). Chloroplast ultrastructure was analyzed using transmission electron microscopy. As shown in Fig. 4C, the chloroplasts of M18 leaves were found to have a more spherical shape and contained many fewer thylakoid membranes. This thylakoid membrane deficiency was especially apparent in the grana stacks, which were severely disrupted. In addition, fewer starch granules were found in M18 chloroplasts when observed under the microscope with low expansion (data not shown), which suggests that the photosynthetic activity of M18 chloroplasts may be weakened.

3.3. PSII activity and the intersystem electron transport process are inhibited in M18 plants

Based on the observation that the thylakoid membrane structure of M18 chloroplasts was severely disturbed, we were interested in how photosynthesis might be affected in M18 plants. The ratio of variable fluorescence to maximum fluorescence (F_v/F_m) measured in dark-adapted plants reflects the maximum capacity of the photochemical reactions of PSII [38]. Under normal growth conditions, the F_v/F_m value in M18 plants was approximately 13% lower than in WT plants (0.717 ± 0.018 and 0.829 ± 0.006, respectively), which reveals that the PSII reaction center remains comparatively active in

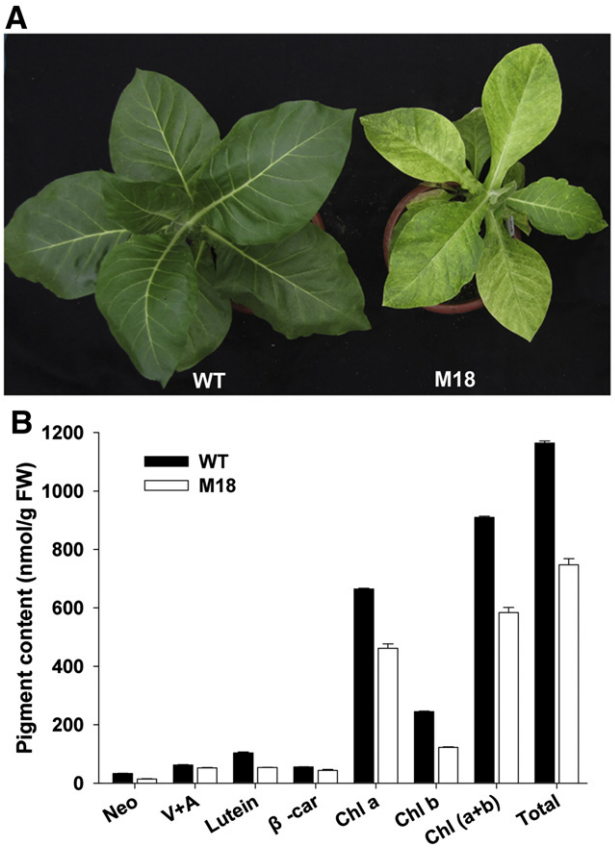

Fig. 3. A, Phenotype comparison of WT and M18 tobacco plants grown for 4 weeks under normal conditions in the greenhouse. B, Pigment composition of developed leaves from WT plants (filled bars) and M18 plants (open bars). Pigment content was expressed as nanomoles of pigment per fresh weight (nmol/g). Neo, Neoxanthin; V + A, Violaxanthin plus Antheraxanthin; β-car, β-carotene. Data are means ± SD from four independent measurements. All pigment components compared between WT and M18 plants exhibited statistically significant differences in their levels ($P < 0.01$).

M18 chloroplasts despite their thylakoid membrane deficiency. However, light response analysis showed that the actual PSII photochemical efficiency (ΦPSII) values measured in M18 plants were much lower than those of WT plants (Fig. 5A), which indicates a severe impairment of PSII activity under light exposure in the M18 plants. This could be explained to some extent by inefficiency in the photochemical quenching process in the transgenic plants (Fig. 5B). Significantly lower qP values (and, consequently, higher 1-qP values) were measured under light exposure in M18 plants, which signify a substantial accumulation of the reduced electron acceptor Q_A^-. This accumulation in turn indicates that electrons released by PSII photochemical separation accumulate in the plastoquinone pool and are not efficiently transported downstream. This observation was supported by the results of oxygen evolving activity measurements. When sufficient PSII artificial electron acceptors (DCBQ) were supplied in vitro, the PSII oxygen evolving activities of WT and M18 thylakoid membranes were comparable (195.1 ± 18.4 μmol O_2 mg^{-1} chl h^{-1} versus 209.7 ± 16.1 μmol O_2 mg^{-1} chl h^{-1}), whereas the whole-chain oxygen evolving activity in M18 membranes (50.0 ± 3.7 μmol O_2 mg^{-1} chl h^{-1}) was approximately 52% lower than that in WT membranes (104.3 ± 3.2 μmol O_2 mg^{-1} chl h^{-1}). This reduced activity indicates that the lower levels of PSII electron transport activity found in M18 plants in vivo resulted from inefficient downstream transport of electrons. On the other hand, the non-photochemical quenching (NPQ) process in the M18 plants was also found to be less efficient than in the WT controls (Fig. 5C). Although the initial response of the NPQ process was faster in the M18 plants than in the WT plants when they were subjected to low light (<270 μmol m^{-2} s^{-1}), which indicates that the light utilization efficiency in the M18 plants is lower, the NPQ values in the M18 plants hardly increased as the actinic light intensity was increased, and this implies an inability to dissipate excess light energy.

The block in downstream linear electron transport detected in M18 plants could be attributed to defects either in intersystem electron transport or in downstream electron acceptors, namely the oxidative PSI reaction center chlorophyll, $P700^+$. To identify the specific electron transport defect resulting from MGDG deficiency, PSI function was investigated by measuring the redox kinetics of P700 at 820 nm using a PAM-101 fluorometer. As shown in Fig. 6A, following actinic light irradiation, a much higher ΔA value was detected in M18 plants, which indicates an accumulation of $P700^+$. This is likely to result from inefficient electron transport. However, a clear absorbance change induced by far-red light was observed in M18 plants, and this was similar to the change observed in WT plants, although with a lower amplitude (for quantitative data, see Table S1). Considering that the measurements were made based on an equal leaf area and that M18 cells contained many fewer chloroplasts (Fig. 4A and B), the P700 chlorophyll in the M18 transgenic was, therefore, almost as functional as that of WT plants. To evaluate the electron transport activity from PSII to PSI, measurement of PSII-dependent re-reduction of oxidated P700 was carried out by superimposing a short pulse of white light onto the far-red light background. Fig. 6A shows that the pool of oxidated P700 chlorophyll was almost completely reduced transiently by electrons released from PSII in WT plants, whereas this process was severely disrupted in M18 plants. This points to an inefficiency in intersystem electron transport. Light response curves for PSI were recorded in WT and M18 plants by Dual-PAM-100 (Fig. 6B) and it was found that, compared with WT values, the Y(I) value (the quantum yield of photochemical energy conversion) in M18 plants started to decrease at a much lower actinic light intensity. This decrease was accompanied by a sharper increase in Y(ND) and by steady levels of Y(NA) (data not shown), which is indicative of a severe limitation in the donor side of the system (namely, accumulated $P700^+$ A [30]). Although impaired PSII activity and the consequent limitation in the electron supply for PSI in light-exposed M18 plants might be responsible for the deficiency in $P700^+$ re-reduction, this possibility was excluded by the detection of a more reduced PQ pool in M18 plants (Fig. 5B). Taken together, the presence of functional P700 and substantial electron accumulation in the PQ pool in M18 plants led us to conclude that the exact site in the electron transport process that is impaired by the MGDG deficiency in M18 plants was between the PQ pool and PSI.

The excitation energy distribution between the two photosystems was also found to be affected in plants of the M18 line. Fig. 7 shows low-temperature (77 K) chlorophyll fluorescence emission spectra for thylakoid preparations from WT and M18 plants upon chlorophyll a excitation. The positions of the two major emission maxima at approximately 688 nm and 730 nm, which represent the emissions of the antenna complexes of PSII and PSI, respectively, were not significantly shifted in M18 plants. However, when the emission spectra were normalized using the PSI maximum, a reduction in the distribution of excitation energy to PSII in M18 plants was revealed, which indicates that the antennae of PSII might be more impaired in the M18 transgenic.

3.4. PSII and Cytb$_6$f proteins show reduced accumulation in M18 plants grown under normal light conditions

To understand the molecular basis of the changes in photosynthetic activity in M18 plants, the steady state levels of photosynthetic proteins were compared between WT and M18 samples by immunoblotting (Fig. 8). A remarkable reduction in light harvesting complex II (LHCII) in M18 plants was clearly detected on a Coomassie Brilliant

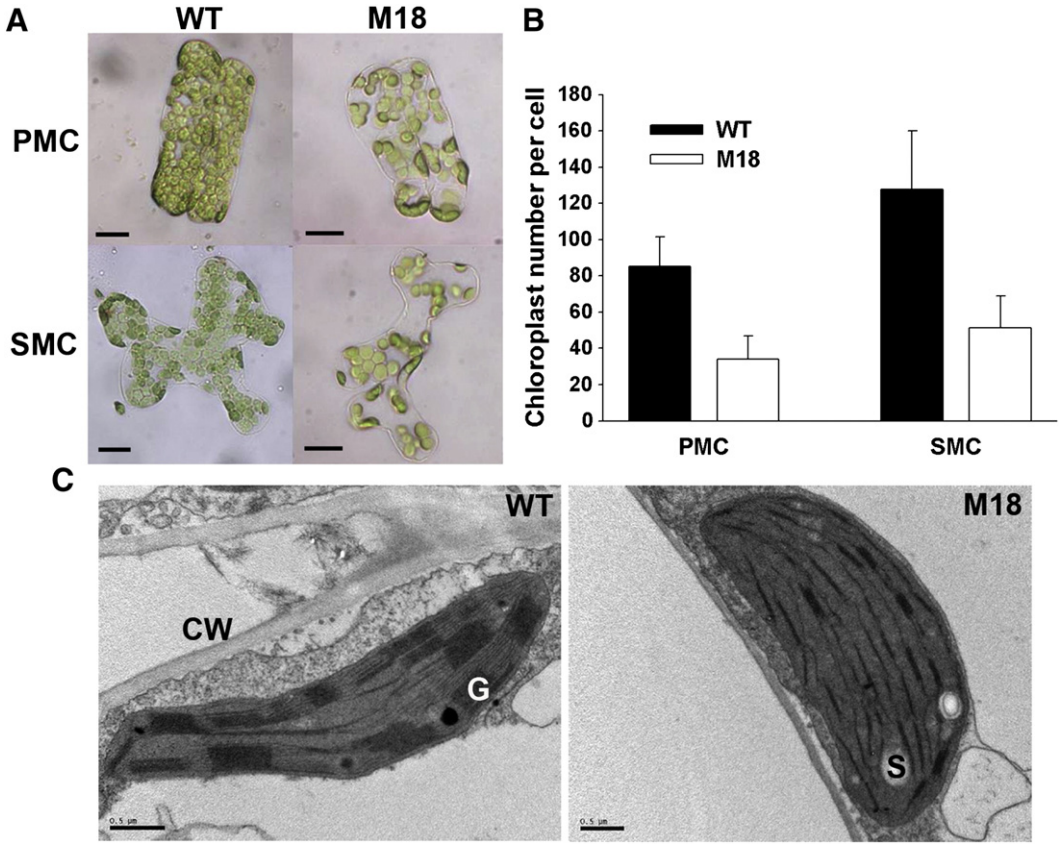

Fig. 4. Chloroplast morphology of leaves from WT and M18 plants grown under normal conditions. A, Representative photographs of mesophyll cells obtained by the maceration of prepared leaf tissues on microscope slides. PMC, palisade mesophyll cell; SMC, spongy mesophyll cell. Scale bar = 10 μm. B, Statistical analysis of chloroplast numbers per mesophyll cell in WT and M18 plants. Data are means ± SD (n = 20 to 48 cells) and statistically significant differences ($P < 0.01$) are shown in both PMC and SMC data. C, Representative electron micrographs of chloroplast ultrastructure from WT and M18 leaves grown under normal conditions. CW, cell wall; G, grana lamella; S, starch granule. Scale bar = 500 nm.

Blue-stained gel (not shown), and immunoblotting analysis showed that it was reduced to approximately 25% of the WT level. To investigate this further, the levels of Lhcb1 and Lhcb2, two major antenna subunits in LHCII, were examined using individual antibodies and the results were approximately in keeping with those of the LHCII analysis. Moreover, similar reductions were also detected in the levels of two minor, peripheral antenna subunits, CP29 and CP26. The levels of the PSII core complex subunits D1, D2, CP47 and CP43 in M18 plants were all found to be reduced to approximately 50% of WT levels. In addition, the levels of PsbO, PsbP and PsbQ, three main subunits of the oxygen evolving complex, were also found to be reduced by approximately 50%. Surprisingly, while the levels of all the aforementioned PSII subunits were reduced in M18 plants, the level of PsbS, which is considered to be necessary for the NPQ process but not for efficient light harvesting and photosynthesis [39], was found to be greatly increased. With regard to PSI, the amounts of PsaA/B and PsaC (indicators of PSI abundance) were not significantly altered in M18 plants, while the levels of four main types of chlorophyll a/b-binding proteins found in light harvesting complex I (LHCI) were slightly reduced. The observation that LHCII was more impaired than LHCI in M18 plants was in line with the results of our excitation energy distribution analysis (Fig. 7).

The block in intersystem electron transport could result from a defect in the $Cytb_6f$ complex. Indeed, immunodetection of cytochrome f, a representative subunit of $Cytb_6f$, revealed a reduction of approximately 50% in the level of this protein in M18 plants versus WT controls (Fig. 8, indicated by an arrow). We further examined the amount of plastocyanin, an important mobile electron carrier in the thylakoid lumen that interacts with $Cytb_6f$ and PSI. It was found that M18 plants contained even more plastocyanin than was present in WT plants, which indicates that the inefficient intersystem electron transport detected in M18 plants is undoubtedly caused by a lack of $Cytb_6f$ activity. In addition, the levels of Ferredoxin:$NADP^+$ reductase (FNR) and ATPase (determined by detection of the CF1β subunit), which catalyze the synthesis of NADPH and ATP, respectively, and the levels of Rubisco [determined by detection of the large subunit of Rubisco (RbcLS)] and Rubisco activase (RCA), which are mainly responsible for the carbon-fixation process, were compared between the M18 plants and the WT controls and no significant differences were found.

To further investigate the structural alterations of the thylakoid complexes, cofactor-protein complexes were solubilized from thylakoid preparations using 1% dodecyl-β-D-maltopyranoside and separated by BN-PAGE (following normalization using chlorophyll, which is the basic active unit for light reaction, as the reference). As shown in Fig. 9A, eight major complexes were resolved, among which six complexes that have been repeatedly detected in previous reports [40,41] were labeled as Bands I–VI, while the remaining two complexes that have not been consistently detected in other studies were marked as Band X and Band Y. All of the complexes were identified by MS/MS identification of proteins separated by two-dimensional SDS-PAGE (Fig. 9B and Table S2). The results clearly showed that the levels of trimeric and monomeric LHCII (Bands V and VI), monomeric PSII (Band III) and the $Cytb_6f$ complex (Band Y) per unit of chlorophyll in M18 plants were all significantly lower than those found in WT control plants. Analysis of two-dimensional SDS-PAGE confirmed that the levels of the subunits resolved from the above complexes were all significantly reduced in M18 plants relative to WT controls (Fig. 9B). Although no obvious difference was observed in the levels of the mixture of monomeric PSI and

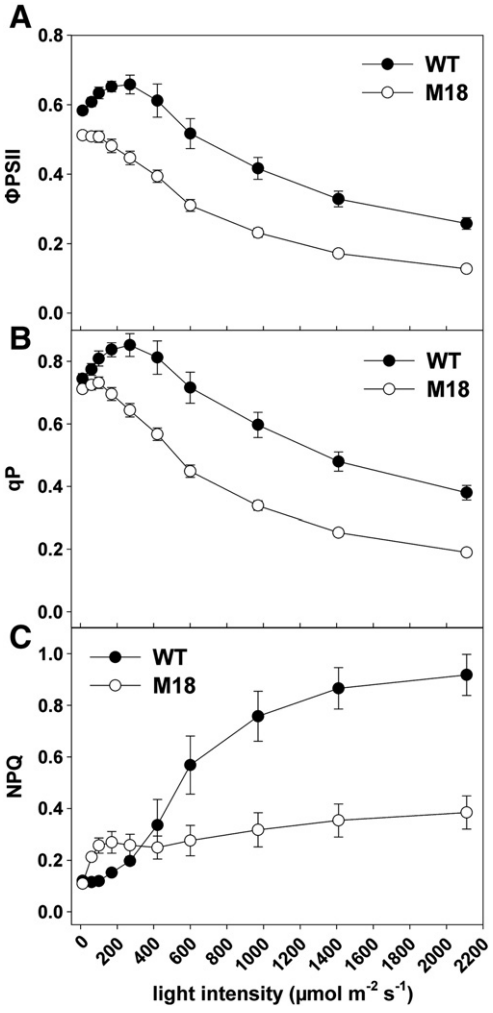

Fig. 5. Chlorophyll fluorescence analysis of leaves from WT and M18 plants grown under normal conditions. A-C, Light response curves of ΦPSII, qP and NPQ in WT plants (filled symbols) and M18 plants (open symbols). Data are means ± SD from five independent measurements. Student's t-tests indicated that the differences in the values of ΦPSII ($P < 0.01$), qP ($P < 0.01$) and NPQ ($P < 0.01$, except for values at 270 μmol m^{-2} s^{-1} and 420 μmol m^{-2} s^{-1}) in M18 versus WT plants are statistically significant. For representative original fluorescence traces of PSII light response curves, see Fig. S1.

dimeric PSII complexes (Band II) on BN-gels, two-dimensional separation revealed that the levels of the PSII core complex subunits CP47, CP43, D2 and D1 were greatly reduced in M18 plants, while the PSI subunits were slightly increased [as was also observed for the PSI subcomplex (Band X)]. In addition, the levels of the ATPase subunits CF1α and CF1β per unit of chlorophyll were also slightly increased in M18 plants. One surprising observation that should be noted is that, while remarkable reductions were detected in the levels of PSII and LHCII in M18 plants, the level of PSII–LHCII supercomplexes (Band I), the native form of the functional PSII unit in vivo, was found to be unchanged (Fig. 9A). This indicates that the higher order complex could be efficiently assembled in M18 chloroplasts. In addition, two-dimensional protein separation (Fig. 9B) showed a proportional reduction in the levels of PSII dimers and monomers in M18 plants, and a similarly proportional reduction was also detected in LHCII trimers and monomers. This was confirmed by immunodetection of the D2 and Lhcb1 proteins on two-dimensional separation gels (data not shown). This suggests that the PSII dimerization and LHCII oligomerization processes were not specifically affected in M18 plants.

3.5. Impairment of the PSII apparatus in normal-light-grown M18 plants is probably the result of cumulative photodamage during long-term light acclimation, while lower accumulation of Cytb$_6$f is a direct structural effect of MGDG deficiency

The results of BN-SDS-PAGE analysis suggested that the reduced accumulation of PSII subunits in M18 plants may not result from biosynthetic feedback inhibition caused by inefficient assembly into higher order complexes. Considering that PSII is the major site of photoinhibition [42], and that leaves with lower chlorophyll concentrations are always more sensitive to photoinhibition [43], we could not exclude the possibility that the impairments of PSII subunits detected in M18 leaves, which contain less chlorophyll than WT leaves (Fig. 3B), resulted from an accelerated degradation of apoproteins under light exposure rather than from direct structural effects of MGDG deficiency. To assess this possibility, we further examined the WT and M18 plants grown under a low light intensity of approximately 100 μmol m^{-2} s^{-1}. This light intensity is quite low for tobacco growth and thus is supposed to exert much less pressure on the PSII apparatus to deal with excess light energy absorbed. Furthermore, we utilized plants grown for 2 weeks in soil (after 4 weeks of growth in flasks) as subjects to exclude any possible cumulative photodamage. Effective silencing of the *NtMGD1* gene and a corresponding deficiency in MGDG were first confirmed in low-light-grown M18 leaves (data not shown). In addition, a corresponding disruption of chloroplast ultrastructure was observed (Fig. S2). Although low-light-grown M18 leaves showed only slightly lower F_v/F_m values than were found in WT leaves (0.792 ± 0.015 versus 0.816 ± 0.002), analyses of the PSII light response and P700 redox kinetics revealed that both PSII activity and the intersystem electron transport process were still inhibited in low-light-grown M18 plants (data not shown). However, immunoblotting analysis showed that although the amount of Cytb$_6$f (determined by measuring Cytf subunit levels) was approximately 50% lower in M18 plants than in WT controls (Fig. 10), which may cause inefficient intersystem electron transport, the levels of accumulated PSII core complex proteins (D1, D2, CP47, CP43 and PsbO) and peripheral antenna proteins (represented by Lhcb1 and CP26) were all found to be comparable between the low-light-grown transgenic line and WT plants. The levels of several PSI subunits (PsaA/B, Lhca1 and Lhca2) and the ATPase subunit CF1β also remained unchanged. These results indicate that the reduced accumulation of PSII subunits detected in normal-light-grown M18 plants was not a direct effect of MGDG deficiency.

To estimate the PSII photosensitivity of WT and M18 chloroplasts, a short-term photoinhibition test was performed on low-light-grown plants by exposing tobacco leaf disks to an irradiation of approximately 500 μmol m^{-2} s^{-1}. As expected, M18 leaves exhibited a faster decrease in F_v/F_m (which is generally used to measure photoinhibition [23]) than WT leaves following the high light treatment (Fig. 11A). Immunoblotting analysis revealed that D1 and D2 protein content declined more quickly in M18 leaves (Fig. 12), which suggests that the PSII core subunits of M18 plants were less stable during photoinhibition than those of WT plants. This may be attributable either to accelerated photodamage or to inefficient recovery of PSII. To distinguish between these two possibilities, the decrease in F_v/F_m during high light treatment of leaf disks pretreated with lincomycin (which blocks the PSII repair process), which is a reflection of the rate of PSII photodamage, was monitored (Fig. 11A). In the presence of lincomycin, the decrease in F_v/F_m was more drastic both in WT and M18 leaf disks. Nevertheless, the rate of the F_v/F_m decrease in M18 disks was found to be significantly faster than in WT disks, confirming that M18 plants exhibit an accelerated rate of photodamage compared with WT controls. To verify whether the PSII recovery process was affected in M18 plants, the recovery of the F_v/F_m values was monitored in WT and M18 leaves after 4 h of

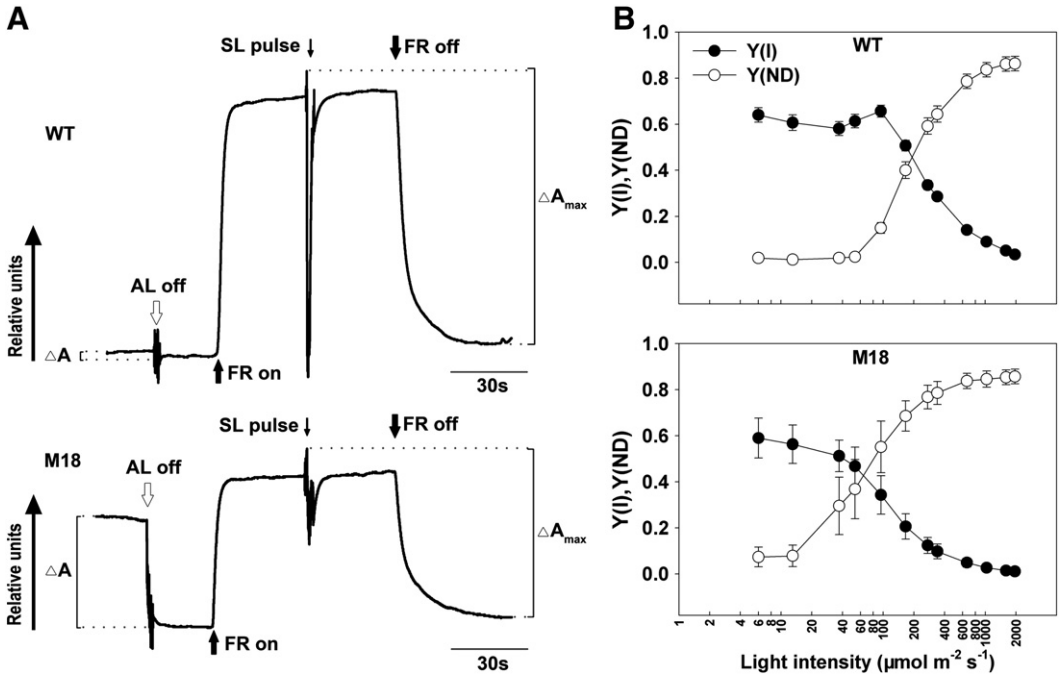

Fig. 6. Determination of P700 function and intersystem electron transport activity in leaves from WT and M18 plants grown under normal conditions. A, Redox kinetics of P700. AL, actinic light (100 μmol m^{-2} s^{-1}); FR, far-red light (720 nm, 24 μmol m^{-2} s^{-1}). ΔA, relative amount of photooxidized P700 under actinic light; ΔA_{max}, relative amount of total photooxidizable P700. Representative traces from six independent experiments are shown here. B, Light response curves of the quantum yield of photochemical energy conversion [Y(I), filled symbols] and the quantum yield of non-photochemical energy dissipation due to donor-side limitation [Y(ND), open symbols] in WT and M18 plants. Data are means ± SD from eight independent measurements.

high light treatment. As Fig. 11B shows, the recovery of F_v/F_m in the M18 leaves was as efficient as that in the WT controls. Therefore, we attribute the susceptibility of M18 PSII to high light exposure mainly to accelerated photodamage rather than to inhibition of the PSII repair process. This conclusion is supported by the results of a photoinhibition and recovery test performed on normal-light-grown WT and M18 plants using a 1000 μmol m^{-2} s^{-1} high light exposure (data not shown).

However, the significantly lower LHCII protein content detected in normal-light-grown M18 plants may not be explained solely by the accelerated photodamage of PSII, as the most vulnerable part of PSII during photoinhibition is the D1 protein of the reaction center rather than the antenna proteins [42]. In fact, the LHCII proteins (immunodetected by anti-Lhcb1 and anti-Lhcb2 antibodies) of M18 plants were found to be as stable as those of WT controls during short-term photoinhibition treatment (Fig. 12).

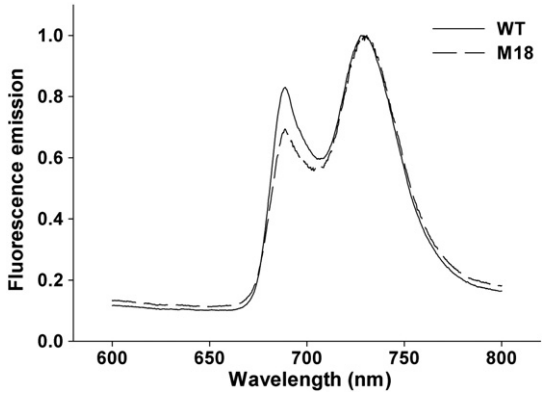

Fig. 7. Low temperature (77 K) chlorophyll fluorescence emission spectra of thylakoid preparations from WT leaves (full line) and M18 leaves (dashed line) upon chlorophyll a excitation at 436 nm. Spectra from WT and M18 samples were normalized to the PSI emission maximum at approximately 730 nm. A representative result from three independent measurements with similar results is shown here.

Taken together, the results described above suggest that only $Cytb_6f$ accumulation is directly affected by MGDG deficiency in M18 plants, whereas the impairments of the PSII core subunits detected in normal-light-grown M18 plants are the result of accelerated degradation due to their lower stability under light exposure. The greatly reduced accumulation of LHCII proteins is likely to result from cumulative photodamage that occurs during long-term light acclimation, although the underlying mechanism is unknown.

4. Discussion

In this study, we utilized the M18 transgenic tobacco plant to investigate the changes in photosynthetic structure and function that are induced by its substantial MGDG deficiency and to explore the underlying mechanism. In M18 plants, the *NtMGD1* gene is always specifically silenced (Fig. 1), which results in a substantial MGDG deficiency. Lipid analysis revealed common features between the lipid profiles of the tobacco M18 line and the Arabidopsis *mgd1* mutants, although some differences were observed. As was found in *mgd1-1* [14] and *mgd1-2* [15] mutants, the reduction in MGDG abundance in M18 plants was accompanied by a relative increase in nonchloroplastic lipid abundance (Fig. 2A), which led to a much lower CL/NCL ratio (Fig. 2B). This finding was in agreement with the reduced numbers of chloroplasts and internal membranes detected in M18 plants (Fig. 4). It is worth noting that the abundance of other chloroplastic lipids was unchanged in M18 samples (Fig. 2A), which implies that the suppression is specific to MGDG biosynthesis. One consequence of this is a large reduction in the ratio of non-bilayer-forming lipids to bilayer-forming lipids in plastids (Fig. 2B), which could be responsible for the abnormality of thylakoid membrane structure in M18 chloroplasts (Fig. 4C). While MGDG, the only non-bilayer-forming lipid in plastids, is considered to be crucial for inducing the curvature of lamellar membranes and, thus, to be important for the formation of grana stacks [4,5], it has also been suggested that LHCII might play important roles in organizing the structure of grana stacks by interacting with MGDG [5,44]. Therefore,

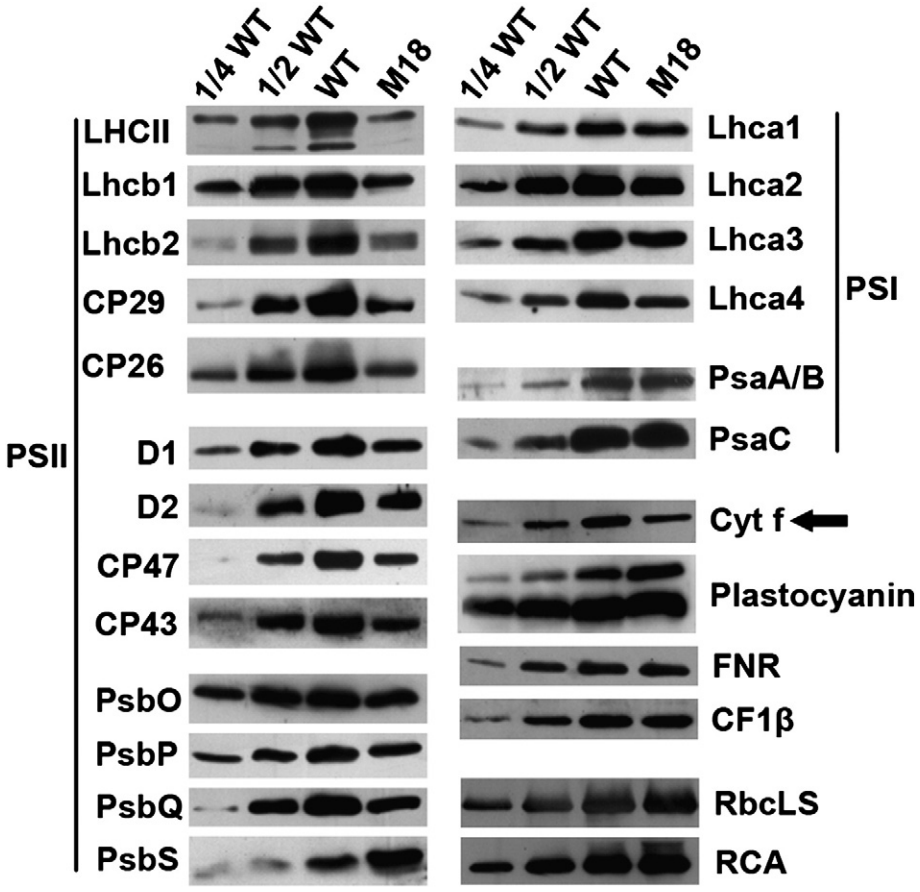

Fig. 8. Immunodetection of photosynthetic proteins in leaves from WT and M18 plants grown under normal conditions. Total proteins extracted from developed leaves were separated on a 15% SDS-PAGE gel containing 6 M urea and were probed by individual antibodies. 1/4 WT, 1/2 WT and WT indicate 5 μg, 10 μg and 20 μg samples of WT proteins, respectively, while M18 indicates a 20 μg sample of M18 proteins. The arrow marks the immunodetection of Cytf. FNR, Ferredoxin: $NADP^+$ reductase; RbcLS, large subunit of Rubisco; RCA, Rubisco activase. Experiments were repeated three times independently and similar results were obtained.

much lower accumulation of LHCII in normal-light-grown M18 plants (Fig. 8) might be at least partly responsible for the poor grana stacking seen in developed chloroplasts (Fig. 4C). However, similarly abnormal chloroplast ultrastructure was also observed in low-light-grown M18 plants (Fig. S2), even though these plants accumulated LHCII levels that were comparable to those of WT controls (Fig. 10). This confirmed that MGDG is indispensable for maintaining chloroplast structure, especially the structure of the grana stacks, and this finding greatly supports previous conclusions from investigations of Arabidopsis mutants [14,15].

Investigations of the photosynthetic properties of M18 plants provided new clues as to the role of MGDG in maintaining linear electron transport activity. PSII light response analysis revealed increased inhibition of PSII activity in M18 plants in response to light exposure (Fig. 5A). Considering that the function of the PSII reaction center in M18 plants was only slightly impaired (reflected by the F_v/F_m values), the inefficient photochemical process in these plants was mainly attributable to the block in downstream electron transport that was revealed by the substantial accumulation of Q_A^- during light exposure (Fig. 5B) and the measurement of oxygen evolving activity. Our analyses of P700 redox kinetics and PSI light response curves (Fig. 6 and Table S1) suggest that the exact site affected in the electron transport pathway of M18 plants was between the PQ pool and PSI. Immunoblotting and BN-PAGE analysis revealed a deficiency in the $Cytb_6f$ complex, relative to either the total protein level or the chlorophyll level, in M18 leaves grown under normal conditions (Figs. 8 and 9). When assayed by immunodetection in plants grown under low light conditions, $Cytb_6f$ accumulation in M18 plants was still found to be greatly reduced compared to that in WT plants (Fig. 10), which suggests that the defect in $Cytb_6f$ is a direct structural consequence of MGDG deficiency and is responsible for the inefficiency of intersystem electron transport in M18 chloroplasts. It is well accepted that the conformation and functional activity of $Cytb_6f$ depend on the charge of the surrounding lipid molecules. Previous investigations in vitro revealed that, among all the thylakoid lipids, MGDG, a non-charged lipid, is the most efficient stimulator of the electron transfer activity of $Cytb_6f$ [45]. Furthermore, the existence of a specific interaction between MGDG and $Cytb_6f$ was recently demonstrated using a biophysical approach [46]. Here, we observed in vivo for the first time that an MGDG deficiency in thylakoid membranes directly leads to a reduction in the accumulation of the $Cytb_6f$ complex. This is probably caused by unstable integration of the $Cytb_6f$ complex into the membrane structure due to its weakened interaction with MGDG. Functionally, besides the defect in the $Cytb_6f$ complex, the MGDG deficient lipid environment could also be responsible for the inhibition of intersystem electron transport activity in M18 plants.

A reduction in the efficiency of photochemical processes in M18 would probably increase the need to dissipate excess light energy through the NPQ process, which is a well-accepted regulatory photoprotective strategy in higher plants [47]. As expected, a faster NPQ response was detected under low light in M18 plants compared with WT plants (Fig. 5C). However, when exposed to higher light levels, the NPQ process in M18 plants was found to be grossly inefficient (Fig. 5C), which was probably due to the lack of carotenoids (Fig. 4B) and the ineffective operation of the xanthophyll cycle in these plants (although this was not examined). Previous in vitro studies have demonstrated that MGDG greatly promotes the de-epoxidation of violaxanthin [48–51]. Furthermore, the importance of

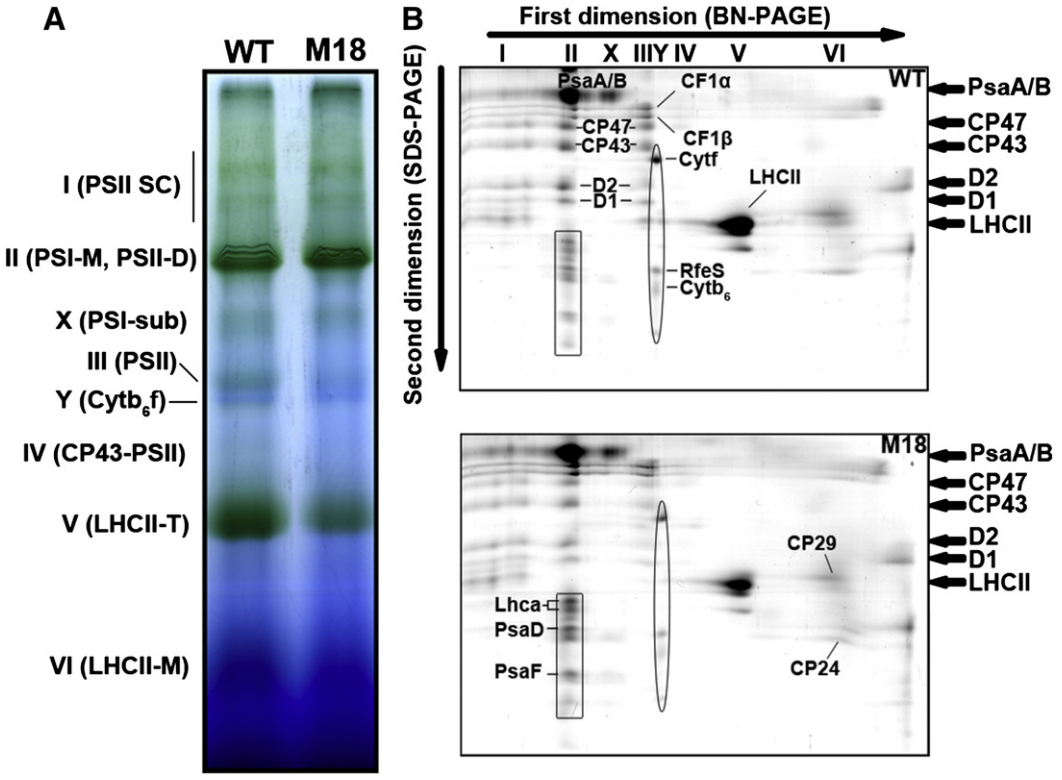

Fig. 9. Analysis of thylakoid membrane cofactor-protein complexes in leaves from WT and M18 plants grown under normal conditions. A, BN-PAGE separation of thylakoid membrane preparations (7.5 μg chlorophyll) solubilized by 1% dodecyl-β-D-maltopyranoside. Eight protein complexes indicated on the left represent the PSII supercomplexes (Band I, PSII SC), the monomeric PSI and dimeric PSII complexes (Band II, PSI-M and PSII-D), the PSI subcomplex (Band X, PSI-sub), the monomeric PSII complex (Band III, PSII), the $Cytb_6f$ complex (Band Y, $Cytb_6f$), the CP43-minus-PSII complex (Band IV, CP43-PSII), the trimeric LHCII complex (Band V, LHCII-T) and the monomeric LHCII complex (Band VI, LHCII-M). B, Two-dimensional separation of protein complexes separated from a BN-gel by 15% SDS-urea-PAGE. The results of protein identification are presented in Table S2 and the names of the proteins are indicated in the figure. Spots enclosed in rectangles correspond to the PSI-associated proteins, while spots enclosed in ellipses correspond to the subunits of the $Cytb_6f$ complex. These experiments were repeated three times independently and similar results were obtained.

MGDG in this process in vivo has also been confirmed by studies of the Arabidopsis *mgd1-1* mutant, in which the inefficient operation of the xanthophyll cycle was found to result from impaired pH-dependent activation of violaxanthin de-epoxidase caused by an increase in the conductivity of the thylakoid membranes (involving leakage of protons from lumen to stroma) under high light conditions. This was induced by an MGDG deficiency of just 42% in this mutant line [19]. It is likely that a similar mechanism also exists in M18 plants and is partly responsible for the inefficiency observed in the NPQ process under high light conditions. One notable feature observed in the tobacco M18 line but not in the Arabidopsis *mgd1-1* mutant is that PsbS protein accumulation was more than two-fold higher in normal-light-grown

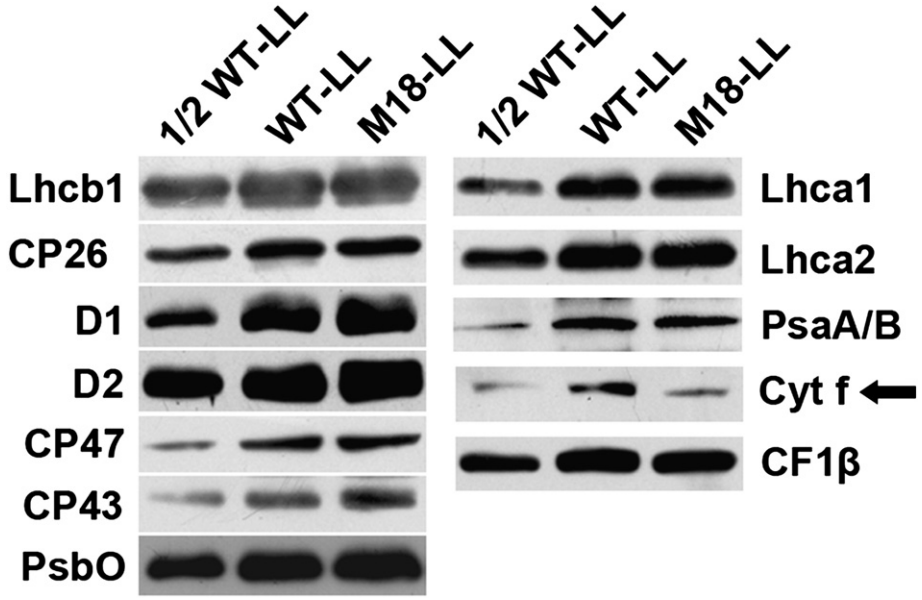

Fig. 10. Immunodetection of photosynthetic proteins in leaves from WT and M18 plants grown under low light (LL) conditions (100 μmol m^{-2} s^{-1}). 1/2 WT-LL and WT-LL represent 10 μg and 20 μg samples of WT proteins, respectively, while M18-LL represents a 20 μg sample of M18 proteins. The arrow marks the immunodetection of Cytf.

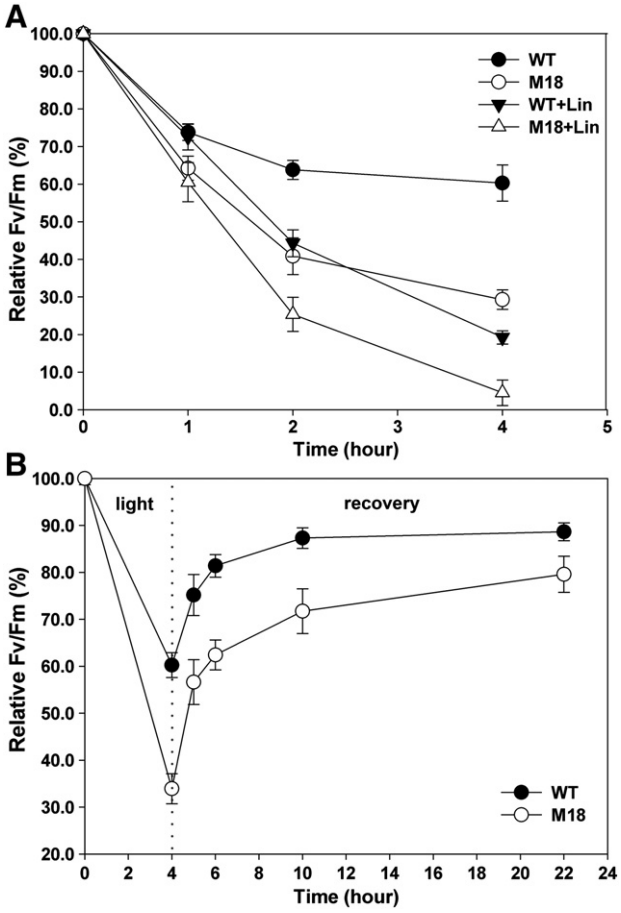

Fig. 11. Estimation of the sensitivity of PSII to photoinhibition in WT and M18 leaves grown under low light conditions (100 μmol m^{-2} s^{-1}). A, Time course of a short-term photoinhibition test in WT leaves (filled symbols) and M18 leaves (open symbols) in which the detached leaves were exposed to irradiance of 500 μmol m^{-2} s^{-1} for 4 h in the absence (circle) or presence (triangle) of 1 mM lincomycin. B, Recovery of F_v/F_m values in WT leaves (filled symbols) and M18 leaves (open symbols) after photoinhibition. Detached leaves were subjected to 500 μmol m^{-2} s^{-1} irradiation in the absence of lincomycin for 4 h continuously, and this was followed by recovery under dim light. All results are expressed as the percentage of the initial F_v/F_m values prior to irradiation (0 h) and values are means ± SD from 8 to 16 measurements at each time point. A representative result from three independent experiments with similar results is shown here.

M18 plants (Fig. 8). This is probably somehow caused by a weak induction of NPQ in M18 plants, as PsbS is considered to be essential for qE (the major fraction of NPQ) [39] and overexpression of PsbS was found to greatly enhance the qE capacity in Arabidopsis [52].

The inhibition of PSII in M18 was found to be more complex than we envisioned. The reduced level of PSII activity observed in low-light-grown M18 plants (data not shown), whose PSII apparatus was not impaired (Fig. 10), indicated that the increased inhibition of PSII activity induced by light exposure in these plants was mainly a side effect of the block in intersystem electron transport. The comparable accumulation of PSII subunits found in low-light-grown M18 plants and WT controls (Fig. 10) suggests that the impairment of the PSII apparatus in normal-light-grown M18 plants (Fig. 8) is not a direct structural effect of MGDG deficiency. Photoinhibition and recovery tests (Fig. 11) revealed an increased sensitivity of PSII to photoinhibition in M18 plants that is primarily due to accelerated degradation of PSII core subunits under high light conditions (Fig. 12). It has been suggested that leaf chlorophyll concentration is a crucial factor in determining the susceptibility of leaves to photoinhibition, and leaves with lower chlorophyll concentrations are always more sensitive to photoinhibition [43]. Therefore, the increased sensitivity to photoinhibition observed in M18 plants (Fig. 11) is most likely a result of their greatly decreased chlorophyll concentration (Figs. 3 and 4) rather than an intrinsic property of PSII. Nevertheless, we cannot rule out the possibility that reduced levels of $Cytb_6f$ and the inefficient NPQ process are contributing factors in the increased sensitivity to photoinhibition seen in M18 plants. The Q_A^- accumulation caused by the block in intersystem electron transport in M18 plants is predicted to slow down the charge stabilization reaction of the primary charge separated state $P680^+$•Phe^-• and thus facilitate the production of $^3P680$ molecules by recombination reactions, which thereby lead to the formation of singlet oxygen ($^1O_2$) and cause PSII protein damage [53,54]. On the other hand, it is believed that NPQ can help decrease the excitation pressure in PSII and provide protection against electron transport-mediated photodamage by dissipating excess light energy before it can reach the PSII reaction center [54]. This activity means that inefficient NPQ under high light conditions could also be somewhat responsible for the fast photoinhibition effect seen in M18 plants. Given that photoinhibition of PSII by visible light is a very complex event which is thought to operate through a dual mechanism in leaves [55], we cannot make further inferences about the mechanism of

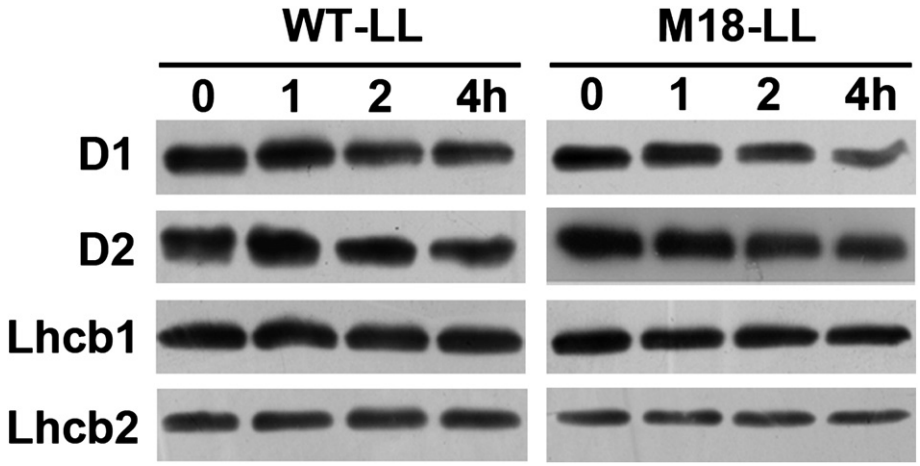

Fig. 12. Estimation of the photostability of PSII proteins in WT and M18 plants grown under low light conditions (100 μmol m^{-2} s^{-1}). Total protein samples were extracted from detached leaves that had been subjected to 500 μmol m^{-2} s^{-1} irradiation in the absence of lincomycin for 0 h, 1 h, 2 h or 4 h, and the PSII protein content was determined by immunoblotting analysis. A representative result from three independent experiments with similar results is shown here.

the faster photoinhibition in M18 plants without further evidence. Nevertheless, according to our results, it is reasonable to attribute the lower accumulation of the PSII core subunits in normal-light-grown M18 leaves (Fig. 8) to the occurrence of net photoinhibition (i.e. faster PSII inactivation than repair) during long-term growth under relatively high light conditions, because the rate constant (k_{PI}) of the damaging reaction of photoinhibition (a first-order reaction [23]) is considered to show an almost direct correlation with light intensity or excess absorbed irradiance [53,55].

Interestingly, the PSII peripheral antenna proteins were found to be more impaired than the proteins of the core complex in normal-light-grown M18 plants (Fig. 8). This explains the greatly elevated Chl a/Chl b ratio in these plants (Fig. 3B), as Chl b is considered to be exclusively associated with the light harvesting complexes [56]. However, LHCII in M18 leaves was found to be quite stable during the short-term photoinhibition treatment (Fig. 12), which indicates that the drastic loss of LHCII in normal-light-grown M18 plants is probably a consequence of long-term light acclimation. We speculate that a reduction in $Cytb_6f$ complex levels, which results in limited availability of the quinol oxidation site (Q_o) for plastoquinol binding, probably limits the activation of the kinase responsible for LHCII phosphorylation [57]. This may lead to a "state I"-type situation in M18 plants, in which LHCII proteins would be very susceptible to cumulative damage caused by excess excitation energy. It is well known that a dose of excess excitation energy can lead to ^{3}Chl and $^1O_2$ production in the light harvesting antenna before it can reach the PSII reaction center, which consequently causes damage to the LHCII proteins [54]. As chlorophyll molecules in LHCII can gain protection against triplet formation from nearby carotenoids [58], the much reduced levels of carotenoids found in M18 leaves (Fig. 3B) would probably exacerbate the damage event. In addition, inefficiencies in both the qP and NPQ processes in M18 plants are expected to enhance $^1O_2$ production in LHCII [59]. Given that the production of ^{3}Chl and $^1O_2$ in the light harvesting antenna is also expected to show linear light intensity dependence [54], the impairment of LHCII that was detected in normal-light-grown M18 versus low-light-grown plants is to be expected. Another possibility that cannot be excluded by our results is that the integration of LHCII in the thylakoid membrane may be affected by the MGDG deficiency during long-term exposure to relatively high light conditions. This possibility is supported by experimental data that have demonstrated a specific interaction between LHCII and MGDG that is involved in organizing the structure of thylakoids [5,44]. Although more experimental evidence is required to better understand this interesting phenomenon, our results indicate that the photostability of LHCII is affected by MGDG deficiency in M18 plants. It is interesting to note that the greater impairment of LHCII proteins than of PSII core complex proteins in normal-light-grown M18 plants (Fig. 8) leads to a decrease of approximately 50% in the LHCII/PSII CC ratio compared with low-light-grown plants. Although it has been suggested that the small antenna size of plants grown under high light exposure offers little or no protection against photoinhibition [53], we still speculate that this alteration in the stoichiometry of the PSII pigment binding proteins (though it may be passive) may aid the survival of M18 plants under relatively high light conditions. This may be somewhat similar to the corresponding phenomenon seen in sun-exposed chloroplasts after long-term acclimation [60,61], which produce fewer Chl-rich light harvesting complexes per reaction center. In fact, M18 plants can survive even when grown in summer with natural irradiation up to about 2000 μmol m^{-2} s^{-1} at noon, though they appear more chlorotic or even bleached due to more drastic loss of antenna proteins (data not shown).

It is well accepted that the PSI complex is less susceptible than the PSII complex to light-induced damage in vivo, and any inhibition of PSII activity should protect PSI from photoinhibition [62,63]. In fact, compared with WT plants, those of the M18 transgenic line accumulated almost comparable levels of the PSI subunits even when grown under normal light conditions. Taken together, our results suggest that MGDG deficiency in tobacco primarily impairs the $Cytb_6f$ mediated intersystem electron transport process. Interestingly, this conclusion is similar to that drawn from the results of lipase digestion experiments reported by Siegenthaler et al. [64]. In addition, the results suggest that the MGDG deficiency in M18 plants indirectly affects the photostability of the PSII apparatus, including both the core complex proteins and the light harvesting antenna, and that this is probably mediated by multiple factors. This phenomenon is of great interest as a potential focus of further investigation.

In our study, despite an MGDG deficiency of greater than 50%, neither PSII dimerization, LHCII oligomerization (Fig. 9) nor the PSII repair process (Fig. 11B) was found to be significantly affected in M18 plants. This indicates that the level of "functional" MGDG molecules may not be affected by the suppressed biosynthesis of MGDG in M18 chloroplasts. This suggests that, when limited numbers of MGDG molecules are available, the plant may tend to preferentially utilize the available MGDG molecules as integral lipid molecules bound to the photosynthetic protein complexes. In this way, the basic functionality of the photosynthetic apparatus might be maintained at the expense of the "structural" lipid molecules found in the thylakoid membrane.

Although the M18 tobacco plant has a greater MGDG deficiency than the Arabidopsis *mgd1-1* mutant (53% versus 42%), the impact on the electron transfer chain and the photosynthetic apparatus detected in M18 plants versus *mgd1-1* mutant plants may not be attributed to this greater deficiency. On the contrary, the different effects are more likely to be induced by the uncontrollable and unpredictable distribution of the residual MGDG molecules among the photosynthetic membranes that results from the suppression of MGDG biosynthesis either by gene inactivation or by PTGS. Another possibility is that the differences in the observed effects on photosynthesis result from species-specific differences between the two model organisms. Regardless, the large-biomass M18 tobacco plant with its stronger survival ability may constitute a useful resource for the further investigation of the role of MGDG in photosynthesis.

In conclusion, our studies of the M18 tobacco plant suggest that, besides acting as an essential bulk lipid in the thylakoid membrane, MGDG also plays important roles in maintaining both the linear electron transport process and the photostability of photosystem II. Our findings therefore highlight the active involvement of this, the major lipid in photosynthetic membranes, in the process of photosynthesis.

Supplementary data to this article can be found online at http://dx.doi.org/10.1016/j.bbabio.2013.02.013.

Acknowledgements

This work was supported by the National Natural Science Foundation of China (30870208) and the National Basic Research Program of China (973 plan: 2011CBA00901). We thank Dr. Lixin Zhang and Dr. Congming Lu for their generosity in providing several antibodies and we are grateful to Dr. Lianwei Peng (Institute of Botany, CAS, China) for his helpful discussion. We are also grateful to the two anonymous reviewers for their constructive and helpful comments on the manuscript.

References

[1] M.A. Block, A.J. Dorne, J. Joyard, R. Douce, Preparation and characterization of membrane fractions enriched in outer and inner envelope membranes from spinach chloroplasts. II. Biochemical characterization, J. Biol. Chem. 258 (1983) 13281–13286.

[2] N. Murata, P.A. Siegenthaler, Lipids in photosynthesis: an overview, in: P.A. Siegenthaler, N. Murata (Eds.), Lipids in Photosynthesis: Structure, Function and Genetics, Kluwer Academic Publishers, Dordrecht, The Netherlands, 1998, pp. 1–20.

[3] P. Dörmann, G. Hölzl, The role of glycolipids in photosynthesis, in: H. Wada, N. Murata (Eds.), Lipids in Photosynthesis: Essential and Regulatory Functions, Springer Science + Business Media B.V., Dordrecht, The Netherlands, 2009, pp. 265–282.
[4] M.S. Webb, B.R. Green, Biochemical and biophysical properties of thylakoid acyl lipids, Biochim. Biophys. Acta 1060 (1991) 133–158.
[5] A.G. Lee, Membrane lipids: it's only a phase, Curr. Biol. 10 (2000) R377–R380.
[6] A. Guskov, J. Kern, A. Gabdulkhakov, M. Broser, A. Zouni, W. Saenger, Cyanobacterial photosystem II at 2.9 Å resolution and the role of quinones, lipids, channels and chloride, Nat. Struct. Mol. Biol. 16 (2009) 334–342.
[7] Y. Umena, K. Kawakami, J.R. Shen, N. Kamiya, Crystal structure of oxygen-evolving photosystem II at a resolution of 1.9 Å, Nature 473 (2011) 55–60.
[8] J. Kern, A. Guskov, Lipids in photosystem. II: Multifunctional cofactors, J. Photochem. Photobiol. B Biol. 104 (2011) 19–34.
[9] N. Mizusawa, H. Wada, The role of lipids in photosystem II, Biochim. Biophys. Acta 1817 (2012) 194–208.
[10] M. Shimojima, H. Ohta, A. Iwamatsu, T. Masuda, Y. Shioi, K. Takamiya, Cloning of the gene for monogalactosyldiacylglycerol synthase and its evolutionary origin, Proc. Natl. Acad. Sci. U. S. A. 94 (1997) 333–337.
[11] P. Dörmann, C. Benning, Galactolipids rule in seed plants, Trends Plant Sci. 7 (2002) 112–118.
[12] K. Awai, E. Maréchal, M.A. Block, D. Brun, T. Masuda, H. Shimada, K. Takamiya, H. Ohta, J. Joyard, Two types of MGDG synthase genes, found widely in both 16:3 and 18:3 plants, differentially mediate galactolipid syntheses in photosynthetic and nonphotosynthetic tissues in *Arabidopsis thaliana*, Proc. Natl. Acad. Sci. U. S. A. 98 (2001) 10960–10965.
[13] C. Benning, H. Ohta, Three enzyme systems for galactoglycerolipid biosynthesis are coordinately regulated in plants, J. Biol. Chem. 280 (2005) 2397–2400.
[14] P. Jarvis, P. Dörmann, C.A. Peto, J. Lutes, C. Benning, J. Chory, Galactolipid deficiency and abnormal chloroplast development in the Arabidopsis MGD synthase 1 mutant, Proc. Natl. Acad. Sci. U. S. A. 97 (2000) 8175–8179.
[15] K. Kobayashi, M. Kondo, H. Fukuda, M. Nishimura, H. Ohta, Galactolipid synthesis in chloroplast inner envelope is essential for proper thylakoid biogenesis, photosynthesis, and embryogenesis, Proc. Natl. Acad. Sci. U. S. A. 104 (2007) 17216–17221.
[16] P. Dörmann, S. Hoffmann-benning, I. Balbo, C. Benning, Isolation and characterization of an Arabidopsis mutant deficient in the thylakoid lipid digalactosyl diacylglycerol, Plant Cell 7 (1995) 1801–1810.
[17] A.A. Kelly, J.E. Froehlich, P. Dörmann, Disruption of the two digalactosyldiacylglycerol synthase genes DGD1 and DGD2 in Arabidopsis reveals the existence of an additional enzyme of galactolipid synthesis, Plant Cell 15 (2003) 2694–2706.
[18] P. Dörmann, Synthesis and function of the galactolipid digalactosyldiacylglycerol, in: C.A. Rebeiz, C. Benning, H.J. Bohnert, H. Daniell, J.K. Hoober, H.K. Lichtenthaler, A.R. Portis, B.C. Tripathy (Eds.), The Chloroplast: Basics and Applications, Springer Science + Business Media B.V., Dordrecht, The Netherlands, 2010, pp. 203–211.
[19] H. Aronsson, M.A. Schöttler, A.A. Kelly, C. Sundqvist, P. Dörmann, S. Karim, P. Jarvis, Monogalactosyldiacylglycerol deficiency in Arabidopsis affects pigment composition in the prolamellar body and impairs thylakoid membrane energization and photoprotection in leaves, Plant Physiol. 148 (2008) 580–592.
[20] J. Luo, G. Wang, Y. Xu, Reduction of monogalactosyldiacylglycerol (MGDG) content in tobacco leaves using RNAi, in: C. Benning, J. Ohlrogge (Eds.), Current Advances in the Biochemistry and Cell Biology of Plant Lipids, Aardvark Global Publishing Company, Salt Lake City, UT, 2007, pp. 16–20.
[21] S. Mongrand, J.J. Bessoule, F. Cabantous, C. Cassagne, The C16:3/C18:3 fatty acid balance in photosynthetic tissues from 468 plant species, Phytochemistry 49 (1998) 1049–1064.
[22] E. Heinz, P.G. Roughan, Similarities and differences in lipid metabolism of chloroplasts isolated from 18:3 and 16:3 plants, Plant Physiol. 72 (1983) 273–279.
[23] D.A. Campbell, E. Tyystjärvi, Parameterization of photosystem II photoinactivation and repair, Biochim. Biophys. Acta 1817 (2012) 258–265.
[24] E. Scotto-Lavino, G.W. Du, M.A. Frohman, 3' End cDNA amplification using classic RACE, Nat. Protoc. 1 (2006) 2742–2745.
[25] E.G. Bligh, W.J. Dyer, A rapid method of total lipid extraction and purification, Can. J. Biochem. Physiol. 37 (1959) 911–917.
[26] G. Wang, Q. Lin, Y. Xu, *Tetraena mongolica* Maxim can accumulate large amounts of triacylglycerol in phloem cells and xylem parenchyma of stems, Phytochemistry 68 (2007) 2112–2117.
[27] S.S. Thayer, O. Björkman, Leaf xanthophyll content and composition in sun and shade determined by HPLC, Photosynth. Res. 23 (1990) 331–343.
[28] K.A. Pyke, R.M. Leech, Rapid image analysis screening procedure for identifying chloroplast number mutants in mesophyll cells of *Arabidopsis thaliana* (L.) Heynh. Plant Physiol. 96 (1991) 1193–1195.
[29] J. Meurer, K. Meierhoff, P. Westhoff, Isolation of high-chlorophyll-fluorescence mutants of *Arabidopsis thaliana* and their characterisation by spectroscopy, immunoblotting and Northern hybridisation, Planta 198 (1996) 385–396.
[30] C. Klughammer, U. Schreiber, Saturation pulse method for assessment of energy conversion in PS I, PAM Appl. Notes 1 (2008) 11–14.
[31] H. Härtel, E. Kruse, B. Grimm, Restriction of chlorophyll synthesis due to expression of glutamate 1-semialdehyde aminotransferase antisense RNA does not reduce the light-harvesting antenna size in tobacco, Plant Physiol. 113 (1997) 1113–1124.
[32] J.F. Martinez-Garcia, E. Monte, P.H. Quail, A simple, rapid and quantitative method for preparing Arabidopsis protein extracts for immunoblot analysis, Plant J. 20 (1999) 251–257.
[33] U.K. Laemmli, Cleavage of structural proteins during assembly of head of bacteriophage-T4, Nature 227 (1970) 680–685.
[34] H. Schägger, Tricine-SDS-PAGE, Nat. Protoc. 1 (2006) 16–22.
[35] L. Peng, J. Ma, W. Chi, J. Guo, S. Zhu, Q. Lu, C. Lu, L. Zhang, LOW PSII ACCUMULATION1 is involved in efficient assembly of photosystem II in *Arabidopsis thaliana*, Plant Cell 18 (2006) 955–969.
[36] R.J. Porra, W.A. Thompson, P.E. Kriedemann, Determination of accurate extinction coefficients and simultaneous equations for assaying chlorophyll a and b extracted with four different solvents: verification of the concentration of chlorophyll standards by atomic absorption spectroscopy, Biochim. Biophys. Acta 975 (1989) 384–394.
[37] O.N. Jensen, M. Wilm, A. Shevchenko, M. Mann, Sample preparation methods for mass spectrometric peptide mapping directly from 2-DE gels, in: A.J. Link (Ed.), Methods in molecular biology, 2-D Proteome Analysis Protocols, vol. 112, Humana Press Inc., Totowa, NJ, 1999, pp. 513–530.
[38] G.H. Krause, E. Weis, Chlorophyll fluorescence and photosynthesis: the basics, Annu. Rev. Plant Physiol. Plant Mol. Biol. 42 (1991) 313–349.
[39] X. Li, O. Björkman, C. Shih, A.R. Grossman, M. Rosenquist, S. Jansson, K.K. Niyogi, A pigment-binding protein essential for regulation of photosynthetic light harvesting, Nature 403 (2000) 391–395.
[40] J. Guo, Z. Zhang, Y. Bi, W. Yang, Y. Xu, L. Zhang, Decreased stability of photosystem I in dgd1 mutant of *Arabidopsis thaliana*, FEBS Lett. 579 (2005) 3619–3624.
[41] X. Sun, M. Ouyang, J. Guo, J. Ma, C. Lu, Z. Adam, L. Zhang, The thylakoid protease Deg1 is involved in photosystem-II assembly in *Arabidopsis thaliana*, Plant J. 62 (2010) 240–249.
[42] E.M. Aro, I. Virgin, B. Andersson, Photoinhibition of photosystem II. Inactivation, protein damage and turnover, Biochim. Biophys. Acta 1143 (1993) 113–134.
[43] E. Pätsikkä, M. Kairavuo, F. Šeršen, E.M. Aro, E. Tyystjärvi, Excess copper predisposes photosystem II to photoinhibition in vivo by outcompeting iron and causing decrease in leaf chlorophyll, Plant Physiol. 129 (2002) 1359–1367.
[44] I. Simidjiev, S. Stoylova, H. Amenitsch, T. Jávorfi, L. Mustárdy, P. Laggner, A. Holzenburg, G. Garab, Self-assembly of large, ordered lamellae from non-bilayer lipids and integral membrane proteins in vitro, Proc. Natl. Acad. Sci. U. S. A. 97 (2000) 1473–1476.
[45] J. Yan, D. Mao, H. Chen, T. Kuang, L. Li, Effects of membrane lipids on the electron transfer activity of cytochrome b_6f complex from spinach, Acta Bot. Sin. 42 (2000) 1267–1270.
[46] G.A. Georgiev, S. Ivanova, A. Jordanova, A. Tsanova, V. Getov, M. Dimitrov, Z. Lalchev, Interaction of monogalactosyldiacylglycerol with cytochrome b_6f complex in surface films, Biochem. Biophys. Res. Commun. 419 (2012) 648–651.
[47] N.E. Holt, G.R. Fleming, K.K. Niyogi, Toward an understanding of the mechanism of nonphotochemical quenching in green plants, Biochemistry 43 (2004) 8281–8289.
[48] D. Latowski, H.E. Åkerlund, K. Strzalka, Violaxanthin de-epoxidase, the xanthophyll cycle enzyme, requires lipid inverted hexagonal structures for its activity, Biochemistry 43 (2004) 4417–4420.
[49] R. Goss, M. Lohr, D. Latowski, J. Grzyb, A. Vieler, C. Wilhelm, K. Strzalka, Role of hexagonal structure-forming lipids in diadinoxanthin and violaxanthin solubilization and de-epoxidation, Biochemistry 44 (2005) 4028–4036.
[50] H.Y. Yamamoto, Functional roles of the major chloroplast lipids in the violaxanthin cycle, Planta 224 (2006) 719–724.
[51] S. Schaller, D. Latowski, M. Jemioła- Rzemińska, C. Wilhelm, K. Strzalka, R. Goss, The main thylakoid membrane lipid monogalactosyldiacylglycerol (MGDG) promotes the de-epoxidation of violaxanthin associated with the light-harvesting complex of photosystem II (LHCII), Biochim. Biophys. Acta 1797 (2010) 414–424.
[52] X. Li, P. Müller-Moulé, A.M. Gilmore, K.K. Niyogi, PsbS-dependent enhancement of feedback de-excitation protects photosystem II from photoinhibition, Proc. Natl. Acad. Sci. U. S. A. 99 (2002) 15222–15227.
[53] E. Tyystjärvi, Photoinhibition of photosystem II and photodamage of the oxygen evolving manganese cluster, Coord. Chem. Rev. 252 (2008) 361–376.
[54] I. Vass, Role of charge recombination processes in photodamage and photoprotection of the photosystem II complex, Physiol. Plant. 142 (2011) 6–16.
[55] R. Oguchi, I. Terashima, J. Kou, W.S. Chow, Operation of dual mechanisms that both lead to photoinactivation of photosystem II in leaves by visible light, Physiol. Plant. 142 (2011) 47–55.
[56] R. Bassi, B. Pineau, P. Dainese, J. Marquardt, Carotenoid-binding proteins of photosystem II, Eur. J. Biochem. 212 (1993) 297–303.
[57] J.D. Rochaix, Role of thylakoid protein kinases in photosynthetic acclimation, FEBS Lett. 581 (2007) 2768–2775.
[58] H.A. Frank, R.J. Cogdell, Carotenoids in photosynthesis, Photochem. Photobiol. 63 (1996) 257–264.
[59] P. Müller, X. Li, K.K. Niyogi, Non-photochemical quenching. A response to excess light energy, Plant Physiol. 125 (2001) 1558–1566.
[60] J.M. Anderson, W.S. Chow, D.J. Goodchild, Thylakoid membrane organization in sun/shade acclimation, Aust. J. Plant Physiol. 15 (1988) 11–26.
[61] L.A. Staehelin, G.W.M. van der Staay, Structure, composition, functional organization and dynamic properties of thylakoid membranes, in: D.R. Ort, C.F. Yocum, I.F. Heichel (Eds.), Oxygenic Photosynthesis: The Light Reactions, Kluwer Academic Publishers, Dordrecht, The Netherlands, 2004, pp. 11–30.
[62] K. Sonoike, Photoinhibition of photosystem I, Physiol. Plant. 142 (2011) 56–64.
[63] C.H. Goh, S.M. Ko, S. Koh, Y.J. Kim, H.J. Bae, Photosynthesis and environments: photoinhibition and repair mechanisms in plants, J. Plant Biol. 55 (2012) 93–101.
[64] P.A. Siegenthaler, C. Giroud, Effects of monogalactolipid (MGDG) depletion on photosynthetic activities in oat thylakoids, Experientia 42 (1986) 658-658.